# Simulation Response of the Optical Modules in the ANTARES Neutrino Telescope

Bachelorarbeit

vorgelegt von
Thomas Heid

Erlangen Centre for Astroparticle Physics
Physikalisches Institut 4
Friedrich-Alexander-Universität
Erlangen-Nürnberg

Gutachter: Prof. Dr. Gisela Anton

Tag der Abgabe: 03. 09. 2012

# Contents

# Chapter 1

# Introduction

Astrophysicists are looking for information about objects in the universe. At first glance it seems that light is a perfect transmitter. It can propagate an infinite distance. But as seen in our daily experience light can be easily absorbed by matter. It is not possible to receive information from objects hidden in dense matter, such as the center of galaxy.
Are there some other possibilities to transmit information from distant objects to us?
In fact there is more cosmic radiation. Mainly it consists of particles. Many of these particles are able to transmit information to the earth. The first cosmic rays to be discovered were protons and heavier nuclei. One big problem of protons in astroparticle physics is their charge, as they are influenced by magnetic fields on the way to the earth. This makes reconstruction of the source direction of protons at the earth difficult or even impossible. The reconstruction is depending on the energy range.
Therefore we are looking for an uncharged particle which reacts with other matter with low probability. One possible candidate is the neutrino. Neutrinos are leptons underlying only gravitation and weak interaction and have thus a low cross-section for interaction with matter. Some interaction models for cosmic acceleration sites predict neutrino production at very high energies, while others predict no neutrino flux. Detecting neutrinos from these sites is of high importance to distinguish between the various models.
As one will see in chapter 3, a large detector is necessary to detect these high energy neutrinos. The neutrinos are detected indirectly by muons emitting Cherenkov radiation. The photons produced through Cherenkov radiation are detected by photomultipliers housed in a glass sphere, the so-called Optical Modules. The topic of this bachelor thesis is to simulate the response of the photomultiplier and read-out electronics of these Optical Modules.
A simulation of the detector is necessary due to the complexity of the detection process. It cannot be described by a fully analytical treatment.

# Chapter 2

# High energy neutrino astrophysics

The ANTARES neutrino telescope detects ultra-high energy neutrinos. This introductory chapter will deal with the question: How can neutrinos be produced and what type of particle is the neutrino?

## 2.1 Basic aspects of neutrinos

Neutrinos are leptons. There are three families of leptons as seen in formula 2.1. Each neutrino in the first line has its corresponding electron-like lepton partner in the bottom line. Additionally, for each particle there is a corresponding antiparticle. But it is not clear until now, if neutrino and antineutrino are different particles indeed or if they are Majorana particles, i.e. the particle is its own antiparticle.

$$\begin{pmatrix} \nu_e \\ e^- \end{pmatrix} \begin{pmatrix} \nu_\mu \\ \mu^- \end{pmatrix} \begin{pmatrix} \nu_\tau \\ \tau^- \end{pmatrix} \tag{2.1}$$

Like for all particles, the movement of neutrinos is influenced by the gravitational force.
Neutrinos are also subject to weak interaction. This force leads to the transformation from electronlike leptons to their corresponding neutrinos and vice versa through the exchange of bosons.
The third way neutrinos can change is the so called neutrino oscillation. There is no additional force underlying this effect. A neutrino of one specific flavour can change into a neutrino of an different family. During oscillation the lepton number is not preserved.[18]

## 2.2 Neutrino creation

In cosmic objects there are several mechanisms to accelerate particles. For the neutrino production one needs especially high energetic hadrons, like protons. If they collide, pions are produced. In the ongoing process, the main reaction to create neutrinos is the pion decay:

$$\pi^+ \rightarrow \mu^+ + \nu_\mu \tag{2.2}$$

$$\pi^- \rightarrow \mu^- + \overline{\nu}_\mu. \tag{2.3}$$

Equation 2.2 decribes the decay to one muon and one neutrino. Equation 2.3 shows the corresponding equation with antiparticles. The branching ratio of these reactions is over 99.99% [17]. So nearly each decay leads to this reaction. Further neutrinos come from the decay of the produced muons, shown in equation 2.4. Here the branching ratio is nearly 100%, too. [17]

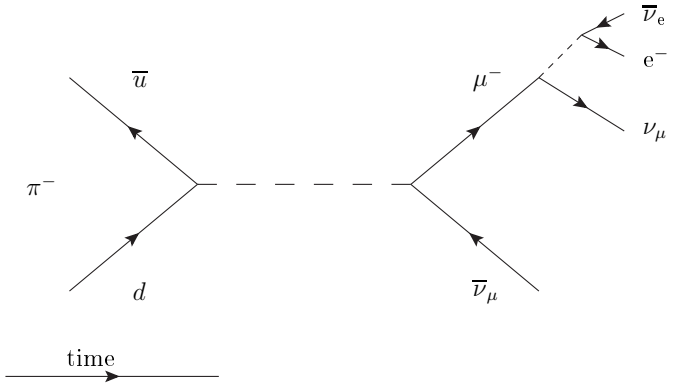


Figure 2.1: Neutrino production with pions

$$\mu \rightarrow e^- + \overline{\nu}_e + \nu_\mu \tag{2.4}$$

In picture 2.1 the whole process is summarized starting from the pion in a Feynman diagram.

## 2.3 Neutrino sources

The mechanisms described above are expected to occur to a large extent in several cosmic objects. The key point one has to look for is an acceleration process to push hadrons to a sufficiently high energy. Some examples of candidates for neutrino sources are listed below.

**Supernova remnants** A first candidate is the supernova remnant. These remnants are the leftovers of dying stars. If the fusion in a star cannot produce any more elements lighter than iron leading to an energy output, the radiation pressure is not high enough to fight the gravitation. The star collapses. Afterwards the material falling to the center of the star is reflected at the formed Neutronstar. The material is accelerated into the space. In the first part, the process produces some neutrinos with low energy, which can be detected as a rise in the countrate of photons in the detector.
On the other hand, there is the shock front of the second part of the process. Particles are accelerated by the so called Fermi acceleration. The neutrinos created within these shocks has sufficient energy to be detected by the detector.

**Gamma ray bursts** Further more, gamma ray bursts might produce neutrinos. According to current models a burst might be the product of the collapse of a super massive star, where a black hole is created. However, the key point is, that there could be two jets back to back in which particles are accelerated in several shock fronts.

**Active galactic nuclei** The third group of objects described here are active galactic nuclei (AGN). This is a typically extragalactic object producing neutrinos. An AGN consists of a super massive black hole of $10^6$ to $10^{10}$ solar masses in the center of a galaxy, which accretes and absorbs surrounding matter. This process creates two jets back to back in which protons can be accelerated for the production of neutrinos.

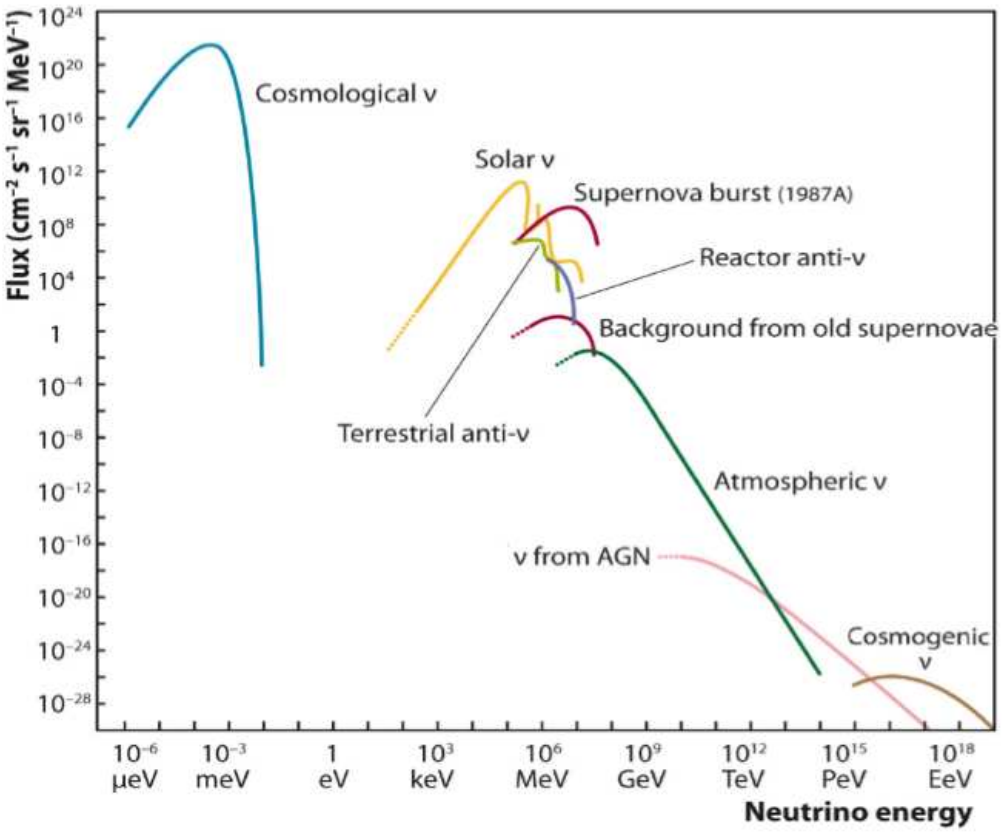


Figure 2.2: Energy spectra of neutrinos from different sources [11]

## 2.4 Atmospheric neutrinos

The so called atmospheric neutrinos are produced in the earth's atmosphere. Cosmic radiation hits particles in the atmosphere, which leads to a shower of particles. The processes described in 2.2 occure as subprocesses and neutrinos are produced. These neutrinos are the dominant source of background for the search for extraterrestrial neutrinos.
To distinguish extraterrestrial neutrinos from atmospheric neutrinos, we are looking for the particle energy. Energy information of the particle can be used, as both types have different energy spectra. The atmospheric spectrum is assumed to follow a power law with index -3.7. For cosmic neutrinos the index is about -2. In the figure 2.2 one can see this behavior taking the predicted AGN spectrum as representative for cosmic fluxes. For comparison, various other sources of neutrinos are plotted. One can recognize the exess of cosmic neutrinos over the atmospheric background. One problem of this separation is that in high energy regimes of atmospheric neutrinos some other mechanisms also play a role [19]. The graph is a combination of measured data and theory and not understood very well until now.

## 2.5 Reaction for the neutrino detection

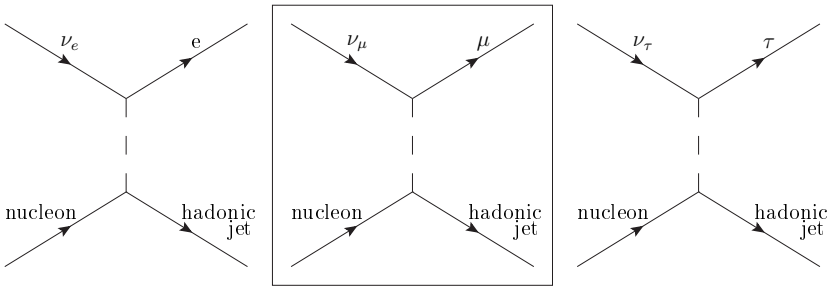


Figure 2.3: possible reactions of neutrinos

As briefly mentioned in the chapters above, neutrinos are very shy particles. One possibility to detect them is an indirect method through charged lepton production.
In the detector volume the neutrinos interact with nucleons and the corresponding lepton is produced. The figure 2.3 shows the three different channels for the detection. The products are charged particles. Charged particles moving faster than light in a medium emit Cherenkov radiation.
For the detection process described in the next chapter one needs a long straight trajectory. In the first channel the electron is easily disturbed by other matter. For example there is the electromagnetic force which leading to an energy loss and scattering. So there is no long straight line. The tau is heavy enough that the forces lead to a smaller acceleration. It can make a straight line, but the particle will decay in a very short time.The last channel, the "golden channel for astronomy" is the neutrino reaction to a muon, shown in the mid part.For further considerations about the detector design one has to care about the fact, that the reactions result from the the weak interaction. The detector should consist of naturally abundant material like water and has to cover a large volume.

# Chapter 3

# The Antares Neutrino Telescope

## 3.1 Detector layout

As seen in the last chapter about the possibility of detection of neutrinos, a large volume is necessary. In order to use naturally abundant target material, ANTARES is located in the Mediterranean Sea in a depth of 2500 meters, 40 kilometers off the coast of Toulon.
In fact ANTARES is operated by a collaboration of about 30 institutes in 8 countries in Europe and North Africa.

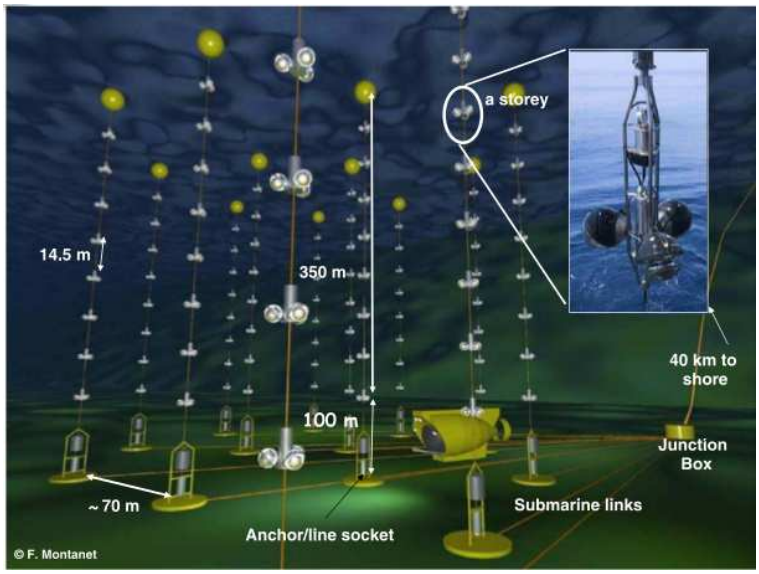


Figure 3.1: Antares neutrino telescope (artist's view) [2]

The whole detector covers an area of $0.1\text{km}^2$ and has a height of about 450m.
As one can see in picture 3.1, the detector consists of twelve detection lines. They are anchored to the sea bottom and pulled upwards by a buoy. Each line is 350 meters long and consists of 25 storeys. The storey is the part of the detector where Cherenkov light is detected. One storey mainly consists of three glass spheres. They are called the Optical Modules (OM). In picture 3.2 an Optical Module is shown. The Optical Modules are looking downwards under an angle of 45°to the ground. Using this arrangement the detector is optimized thus that it sees primarily muons from neutrinos coming out of the earth, e.g. no atmospheric muons as these are absorbed by the earth. Atmospheric muons react with atoms of the earth. There are 885 such Optical Modules. Optical Modules consist of a photomultiplier, some electronics and sensors. The photomultiplier converts the photon to a charge pulse. The readout electronics are used to digitize pulses and time informations for the reconstruction of muon trajectories

and transfers this data to shore.

Figure 3.2: Optical Module [3]

The lines are not fixed to their position, they can slightly move around their mean position to follow the sea current. It is necessary to localize them. Among others this is done by an acoustic signal every few minutes.

## 3.2 Detection principle

ANTARES detects the neutrinos indirectly. Neutrinos create muons under the reaction with nuclei. The produced muons emit Cherenkov light, as they travel faster than light in water. The light is emitted under an angle $\Theta$ of about 42°. It depends on the refractional index according the equation:

$$\cos\Theta = \frac{c}{v \cdot n}[10] \tag{3.1}$$

with c the speed of light, v the velocity of the particle and n the refractional index. If several Optical Modules detect photons at certain points in time, it is possible to reconstruct the trajectory of the particle. The direction of the muon is nearly the same as the one of the neutrino. For high energetic neutrinos this is a good assumption. The angular resolution of the reconstruction of the reconstructed muon track is about 0.5°[6].
The light has to travel through the water. There is absorption and scattering. Absorption only decreases the amount of light which can be detected. On the other hand scattering can disturb the path of light, which can pose a problem for muon track reconstruction. In the range of wavelength of the Cherenkov light at the ANTARES site the absorption length lies between 50 and 70 m. The scattering length is in the range from 230 to 300 meters. [4]

## 3.3 Photon background

The detector is looking for light of muons, but there is other light in the sea, too.
Part of this light is out of bioluminescence, that means bacteria, emitting light, or some animals with luminous effects. Further there is the decay of Kalium-40 emitting light in the frequency band of the Cherenkov radiation. The emission of light can be localized or widely distributed over the whole detector. The distributed sources adds to the noise of the detector. On the other hand localized sources can be filtered out from the data.
It is assumed that the background consists mainly out of 1 p.e. hits. These hits can be used for studies of background only events, so-called Minimum Bias event. These events are captured when the PMT signal is digitized at random times, without any muon being detected within the same timeslice. [9]

# Chapter 4

# Physics of the optical module

As shown, the ANTARES neutrino telescope consists of 885 Optical Modules. In this chapter the main features for these modules will be explained in more detail.

## 4.1 Photomultiplier

The first step from the photon of the Cherenkov radiation to digital data is the photomultiplier converting the photon to a charge pulse.

### 4.1.1 Functional principle of photomultipliers

Photomultipliers are one of the most sensitive photon detectors. They can detect single photons. Figure 4.1 shows a sketch of a photomultiplier tube. The light is coming from the left. The first interaction in the detector is located at the photo cathode. The photons cause the photoelectric effect. Electrons leave the cathode because they are kicked out by the energy of the photon. It is important to mention that there is a threshold to leave the cathode, called the working function. To be sensitive to some specific light, its frequency has to be high enough to offer enough energy for the work function. In ANTARES the used cathode material is Bialkali [12]. The spectral sensitivity is in the range from 300 nm to 650 nm. The maximum sensitivity is at a wavelength of 420 nm [12].

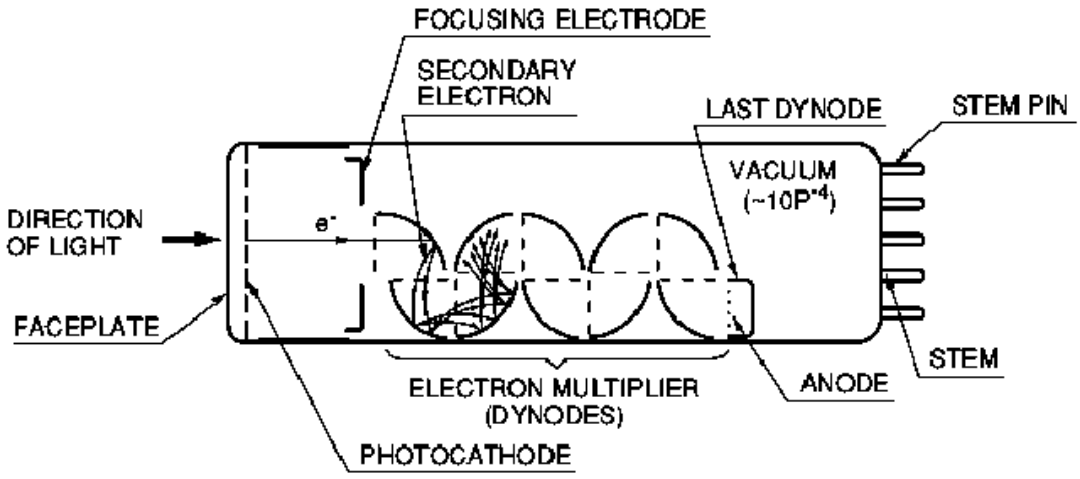


Figure 4.1: Schematic diagram of a photomultiplier tube [12]

The free electron moves towards the first dynode. The dynodes are charged positively to attract the electrons. As seen in the picture the incoming electrons cause an cascade of secondary

electrons. These electrons move to the next dynode. Each dynode has a positive voltage respectively to the one before. In that manner the electrons are accelerated from one electrode to the next. Finally the incoming electron flux is amplified. The anode collects the final flux of secondary electrons. [16]
With some electronics described later it is possible to measure a signal of voltage according to the amplified electrons.
As one can see in figure 4.1, different electrons travel on slightly different paths through the photomultiplier. At the end, not all electrons are at the anode at the same time. There is a so called transit time spread. The more electrodes are used the wider the resulting time spread. The distribution of the time of detection is not as sharp as the time distribution of the incoming photons. Concluding one has to use as few dynodes as possible. On the other hand you have to use as many dynodes as necessary to amplify the signal. Currently we use photomultipliers with 14 dynodes, which leads to a transit spread time of 3.3 ns [12]. For the process of reconstruction, the time from the entering of the photon to the detection at the anode is of importance. This time is called electron transit time. [16]

### 4.1.2 Types of pulses

Additionally to these main-pulses, spurious pulses can be created. We classify them into several groups according to their time of arrival. In figure 4.2 you can see the different paths of electrons and photons through the photomultiplier. Photons are symbolized as waved lines and other particles like electrons as lines.

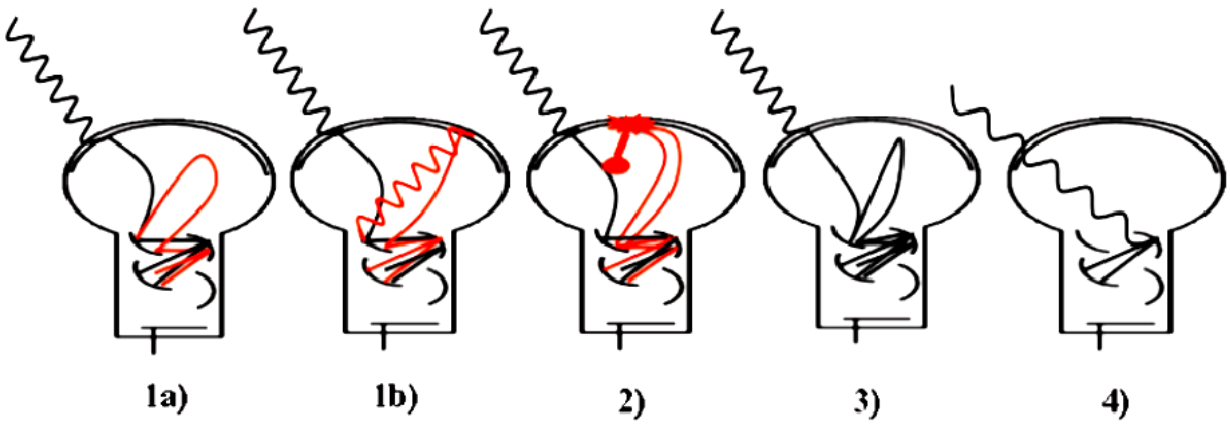


Figure 4.2: Pulse origin in a photomultiplier [14]

After-pulses type 1 appear up to 80ns after a main-pulse. 1a) shows one secondary electron escaping from the dynode, but it does not move directly to the next dynode. The electron hits the first dynode again and causes an additional cascade.
After-pulses type 1 are also caused by photons emitted on the dynode as shown in 1b). This photon itself can react with the photo cathode to start an additional process in the photomultiplier, leading to a new pulse.
The type 2 of after-pulses can be traced to the ionization of gas atoms in the photomultiplier. The mechanics are shown in picture 4.2 2) This type appear between 80ns and 16$\mu$s after the main-pulse.
Further there is the late-pulse (see 3)). In this case the primary electrons do not lead to secondary electrons at the first contact. It scatters. Finally it reaches the dynode again so it creates a cascade of electrons.
The fourth way of creating a pulse is the pre-pulse. The pulse is created by a direct interaction between the incoming photon and the dynode. Because the light is faster in the photomultiplier

than the electron, the pulse appears earlier. The pulse has a lower charge than a main-pulse. [14]

## 4.2 Analogue Ring Sampler

The Optical Modules deliver an analogue and continuous signal. Caused by a limited capacity of data flow the amount of data has to reduced. One has to digitize the data. Further one does not need the signal from all times. One only needs data out of periods when photons are detected. For all these purposes there is the Analogue Ring Sampler (ARS).
The ARS has two main functionalities: It can sample the whole waveform and it can capture the integrated charge of a pulse and the time of detection. ANTARES works only with the second mode in daily work.
The functioning principle is the following: The Optical Modules deliver a continuous voltage, the signal. When the signal crosses a threshold, typically one third of a common one photo-electron hit, the pulse integration is started. Additionally the ARS creates a time stamp. The electric circuit integrates the signal over a time of 25 ns.[5]. These information can be held in the module. After it has collected up to 16 SPE-hits, the module sends the data package to coast. [5].
Because one has to read out and send the data, there is a dead time. In this time no other pulse can be detected. To reduce this time of blindness we use two ARS chips. [5].

# Chapter 5

# Analysing pulse shapes

As basis for simulation of new random pulse shapes I use measured waveforms from Gauchet Lucien and Creusot Alexandre. These waveforms were measured with the same setup [8] as used in the ANTARES neutrino telescope.

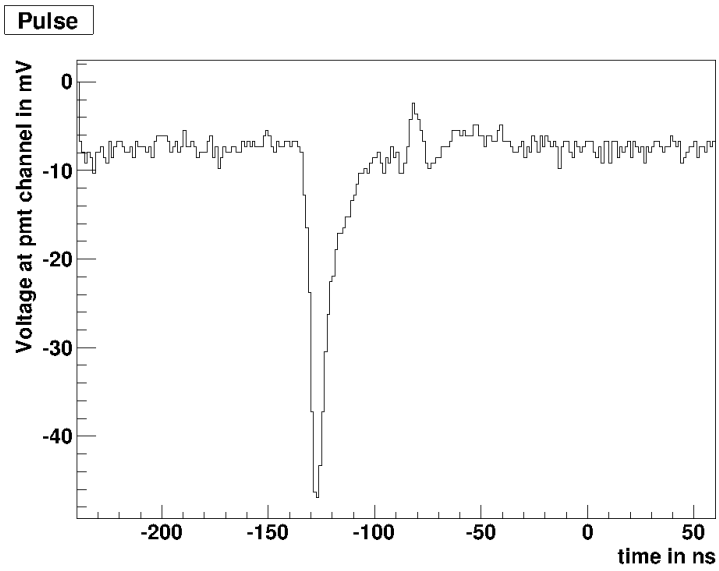


Figure 5.1: Example of a waveform

The idea of the simulation is to characterize a PMT pulse shape by some characteristic values. If one considers figure 5.1, one easy way is obvious. You can fit a function to the pulse shape. The free parameters of the function are the characterizing values. The first aim is to get a distribution of these values. In the simulation process, one can draw values out of these distributions.

Further on I must take into account that there can be correlations between different parameters. If I draw out of these correlated distributions, we do not get the right multivariate distribution over all parameters as you will see in chapter 5.5.

In the next two chapters I go through the analyzing and generating process of the pulses. First one has to make some preparation on the pulses due to the shift of the origin of coordinate system. Then one can perform a fitting process to get characterizing numbers of the pulses. These numbers could depend on each other, so one has to think about solutions to receive independent parameters. There are many possibilities to simulate new pulses. In the next chapter I will tell how the simulation of new pulses is performed.

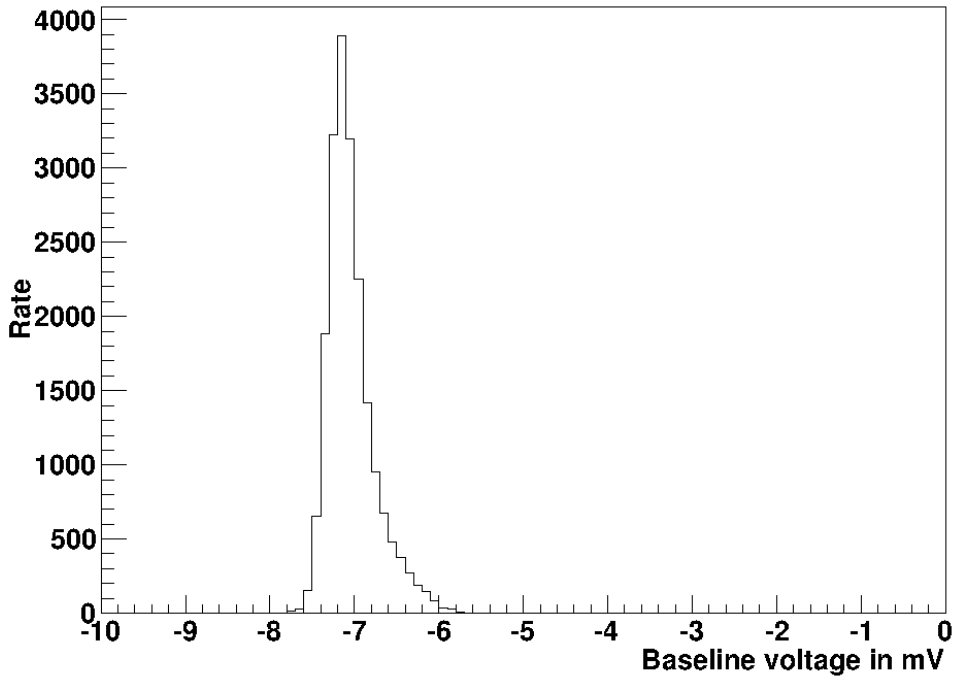


Figure 5.2: Distribution of the meanvalue of the baseline

## 5.1 Preparations

I prepared the waveforms in a way that I subtracted the background. We are not interested in the background, we are interested in the pulse. For this purpose you need the mean value of the baseline. In Figure 5.2 one sees the distribution of the baseline in the single waveforms. As it is a small distribution we take the mean value of the distribution, as a baseline for all values.

The next preparation concerns the time axis. As can be seen in figure 5.1, the range covered by pulses along the time axis was from -240 ns to 60 ns. For simulation purposes it is necessary to estimate a zero point. The choice does not play a big role, because it only causes an time offset in final results. But we have to think about it and make a decision. As seen, there are several kinds of pulses. The main-pulse delivers the main contribution. So we take the mean value of the time of maximum amplitude of these pulses for the zero point. In Picture 5.3 one can see the resulting distribution. Again it is a very sharp distribution, which comes out of the small transit time spread of the photomultiplier.
Finally we shift the waveforms for -7.36 mV in the voltage dimension and 126.9 ns in time. Further I take the absolute value, because it was easier to find fit parameters for ROOT.

## 5.2 Separating different kinds of pulses

As mentioned above, there are several kinds of pulses. We want to simulate these in different ways. It is not necessary to simulate all groups separately. It is sufficient to use two groups. First there are single pulses. In this group are main-pulses, pre-pulses and late-pulses.
On the other hand there are double pulses, that means one pulse followed by an other pulse, like after-pulses. Picture 5.4 and 5.5 shows two typical pulse shapes out of the two groups.
One can imagine that there are a number of different ways to get double pulses and single

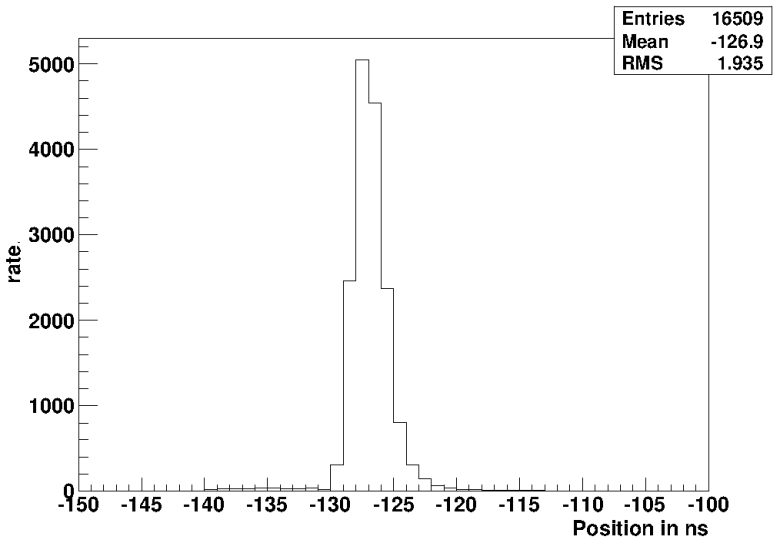


Figure 5.3: Distribution in time of the main-pulses

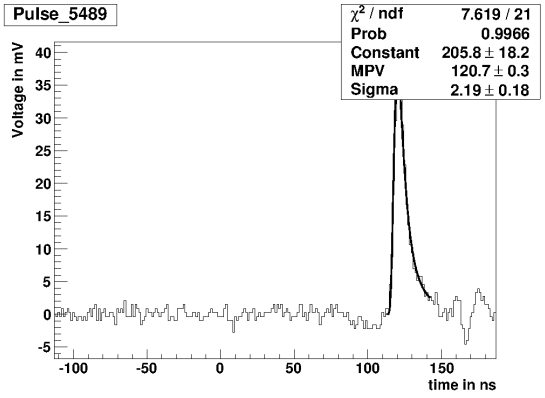


Figure 5.4: Single pulse

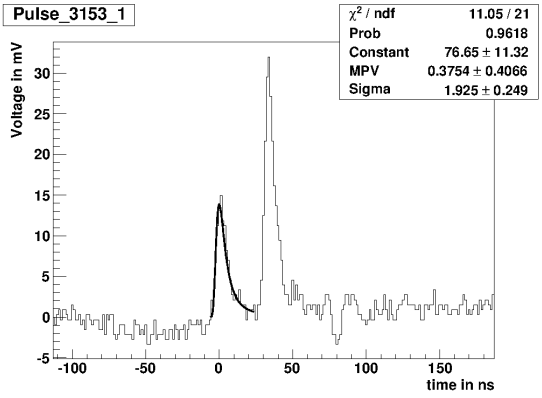


Figure 5.5: Double pulse

pulses. All the necessary information is captured in the fit parameters. At the final simulation I will decide under certain probabilities if I want a double or a single pulse. Afterwards pulse parameters are created. A new pulse is simulated.
Within the double pulses I will symbolize first or second pulses by a corresponding number at the parameter name when it is not clear which is meant.

## 5.3 Search for pulses

First I have to find the pulses in the data. Further, to achieve good results it is the best approach to restrict the range of fitting, otherwise features in the background can dominate the fit. We are looking for a range in which the main contribution to the signal is the pulse itself. I classify a pulse by voltage over mean value. The signal has to rise above a threshold of 5 mV. This threshold is approximately about one fifth of 1 pe pulse. Because of some disturbances bigger than the threshold, I am looking for long enough pulses. In fact I use a threshold of 10 ns here. The start of the fit period is set to 6 ns before the signal rises above the threshold, so I receive the whole pulse rising out of the background.

One other problem is receiving the right fit range for narrow pulses like in figure 5.6. Two mistakes occur. First the second pulse is missed, because the voltage is not under the threshold again.
Secondly the fit range would be too big and the fit is wrong due to the fitprocess trying to fit the function on the data with two peaks.

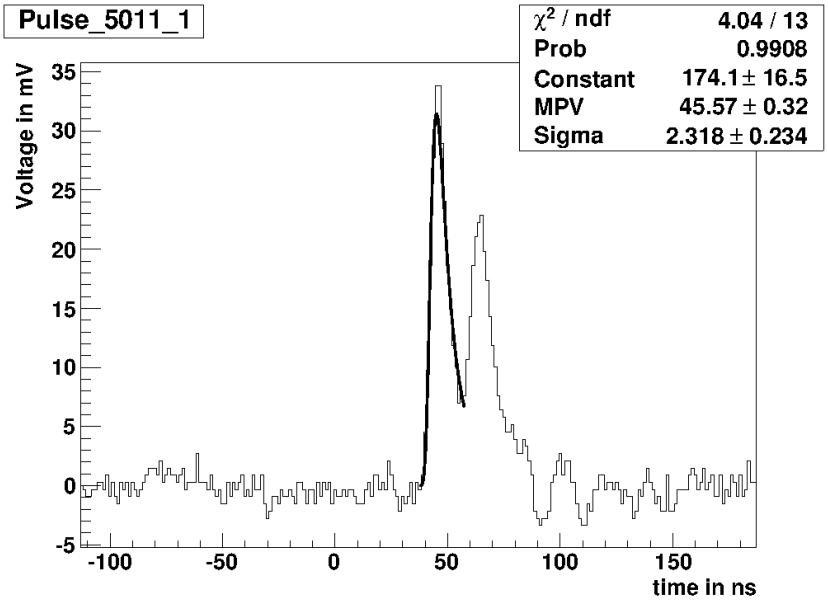


Figure 5.6: Narrow pulses

To avoid the first problem I do not look for the end of the pulse for the fit period. I can assess the time of the pulse. I used 30 ns for the duration of one pulse.
The other problem is solved by looking for a second rise in voltage. If the first pulse decreases a search mode is set into alarm. Now if the voltage is rising again, I wait a small time (here 5 ns) and check if the pulse continue rising. If the second rise is detected, the second pulse is detected.

## 5.4 The fitting process

For a good fit process one has to find a function with the same properties as the data. The main characteristics of the pulse forms are the steep rise at start and the tail at the end. I tested some functions. The first and simplest way is a polynomial function of degree n. The result leads to n+1 free parameters. Each analytical function can be approximate in that manner in arbitrary precision. But there are many free parameters. Other functions are perhaps better suited. The best results are achieved with a landau distribution. It was developed for the energy loss of particles in dense matter by Landau [15]. For the fitting we are using ROOT. Here the calculation of the Landau distribution is adapted from the CERNLIB routine G110 denlan. And the description for the landau distribution of [13] is used.
Figure 5.7 shows a landau distribution fitted to a measured pulse. There are three parameters coming out of the fitting process. First the MPV standing for the approximated time of the maximum amplitude. Secondly there is the Sigma value which describes the width of the pulse. Finally the value called “constant”. It stands for a prefactor of the distribution to get different amplitudes.[20]

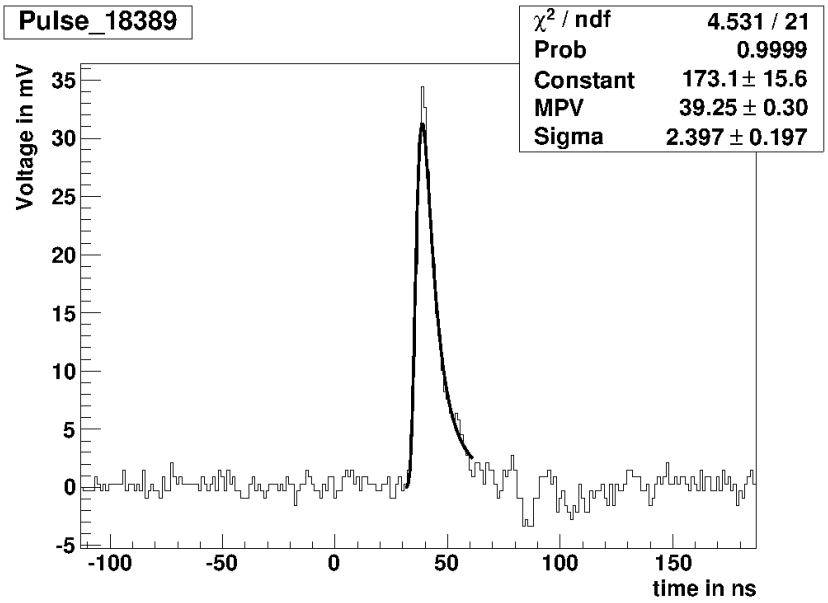


Figure 5.7: Landau distribution fitted to a pulse

The Fitprocess is performed by using the fit routine of ROOT. It is using the $\chi^2$-minimum method. The idea of that methode is to find a minimum of the approximated error

$$E(h^e, h^t)_i = \sum_i \frac{(h_i^e - h_i^t)^2}{h_i^t} \text{ (with } i = 1, \ldots, N). \text{ [1]} \tag{5.1}$$

The formula describes the quadratic deviation between the fit and the data. $h_i^e$ is the measured value of the i-th bin. $h_i^t$ is the value of the theory, here the value of the fitted function at bin i. N is the number of bins the function is fitted.
Finally one receive three fit parameters called constant, sigma and MPV.

**Goodness of fit** The goodness is tested by the $\chi^2$-distribution test. The idea of the test is, that one check if the fit can be achieved by other models with a high probability. A given hypothesis, the generated fit, is refused under a certain significance level. Commonly one tests a theory by a set of measured data.
The used test looks for deviations of the data from the theory. As seen above the data is binned in the time axis, so we can look for deviations in each of the N bins used for the fitting process. Equation 5.2 is the value we get for each bin.

$$E(h^e, h^t)_i = \frac{(h_i^e - h_i^t)^2}{h_i^t} \text{ (with } i = 1, \ldots, N) \text{ [1]} \tag{5.2}$$

$h_i^e$ is the measured value of the i-th bin. $h_i^t$ is the value of the theory, here the value of the fitted function at bin i.
Because negative and positive differences are not to be eliminated by each other, I am using the squared difference. The denominator leads to equal relations between large and small values. Big deviations at big values are not as heavy as small deviations at small values.
Next I sum over all bins and get:

$$y = \sum_{i=1}^{N} \frac{(h_i^e - h_i^t)^2}{h_i^t} \tag{5.3}$$

This value tends to a $\chi^2$-distribution with $k = N-1$ degrees of freedom. One takes an arbitrary value for the significance level, for example 5%. This means that if one refuse the hypothesis there are 5% of distribution underlying the tested hypothesis but have a more extreme $\chi^2$ than the threshold. [1]
Further one can calculate the P-Value. The P-Value stands for the amount of distributions underlying the theory having a more extreme $\chi^2$ than the tested one, e.g. is not fitted as well to the theory as the tested. One see that a high P-value symbolizes a good fit to the data.

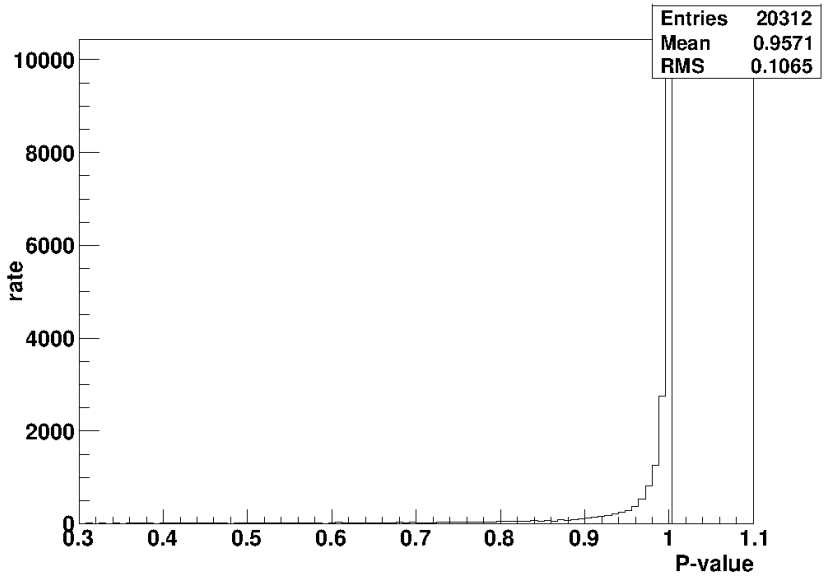


Figure 5.8: P-Value of fitted pulses

In Figure 5.8 you see the distribution of the P-Values of all fitted and used pulses. The values are quite large so I can assume the fit process was mostly successful. I can use the fit parameters for the simulation. I do not have to make a cut on the fits to get rid of the badly fitted functions.

## 5.5 Principal component analysis

The last chapters were dedicated to the search for parameters to characterize the physical data. They are probably not the best choice for getting statements of an underlying physical model. The parameters could be correlated or some could be not of much interest. For example one can image, someone investigate some boxes of a specific material. He is measuring the size and the weight of the boxes. He has two numbers for each box he is investigating. One already realized the size and the weight is correlated, that means the bigger the box the heavier the box.
In our case the final goal was to get independent parameters to be able to draw up new parameters for the simulation of pulses. So we have to look for a method to test and get rid of correlated parameters. Here the principal component analysis (PCA) can be used.
The main goals of the PCA are:

- extracting the most significant data
- getting rid of correlated data

The PCA leads to a linear transformation. The transformation converts measured parameters, called points in the pattern space, into the feature space. One can also perform the transformation the other way round, which is needed for simulation.

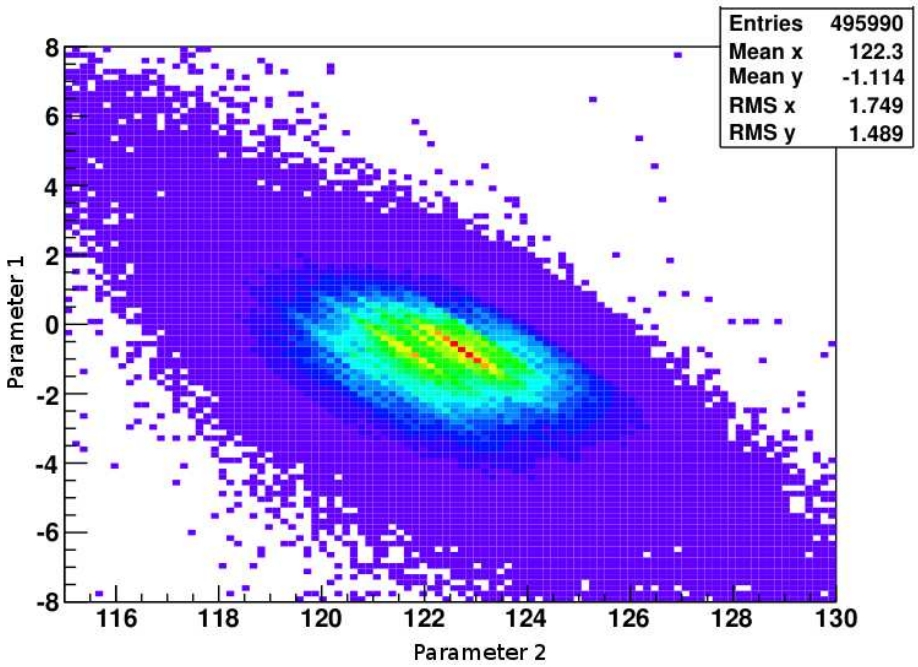


Figure 5.9: correlation in two dimensional data

In figure 5.9 one can see a 2D-Plot of the amount of pulses with a certain combination of the two parameters. They are correlated, recognizable by the inclination of the cloud. The used data is out off a fit process to pulse shapes of different kinds than used finally for this bachelor thesis. If one draws the parameters according to that coordinate distributions, one does not receive the underlying distribution in two dimensions, because they are correlated. We have to find a basis in which the parameters are not correlated.
In this bachelor thesis I took the TPrincipal class of ROOT [21] for this purpose.
What I am looking for are axes of parameters orthogonal to each other. That means they are independent of each other. The used class applies the covariance method to get the new coordinate system. First it is looking for the covariance matrix. It is defined as follows:

$$C = \langle yy^T \rangle \quad \text{with } y = x - \langle x \rangle \tag{5.4}$$

Here x is the point in pattern space and the brackets indicate the mean value. This matrix is a measurement for the linear dependence of the variables. The matrix element $c_{ij}$ of matrix $C$ stands for the correlation between coordinate i and j. The matrix is a generalization of the variance of a one dimensional distribution to a multivariate distribution.
Once the covariance matrix is calculated one can easily get the axis I am looking for. One has to get the eigenvalues and eigenvectors. The eigenvectors $\overrightarrow{e_1}$ to $\overrightarrow{e_n}$ build up the transformation matrix T from pattern to feature space.

$$T = \left\{ \overrightarrow{e_1} \quad \overrightarrow{e_2} \quad \cdots \quad \overrightarrow{e_3} \right\} \tag{5.5}$$

One diagram out of the final result to the above used data is shown in figure 5.10. You see the shape is aligned to the axis.
One can reduce the number of coordinate axes if wished. One has to consider that you loose information, but on the other hand you can reduce your amount of data. Often some values

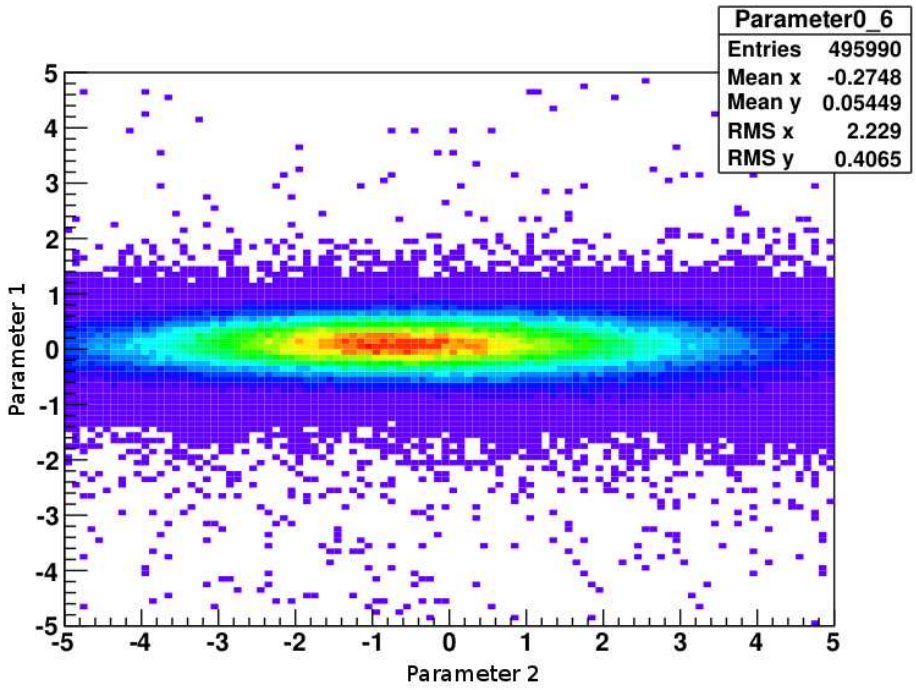


Figure 5.10: Transformed parameters in feature space

are not of interest, like the mass of the boxes in the example above, then you can get rid of that data.
But what data is important and what can we cut? Commonly you sort the eigenvectors by the corresponding eigenvalues. The higher the value the more significant the component. You have to take as many of the components as you want, but starting with the one with the biggest eigenvalue.
A last question is left. When is PCA necessary? If there is no correlation in the data one does not need the PCA. It is not easy to see it in diagrams in all cases. I have already used the covariance matrix. If there are numbers near by zero in nondiagonal elements, one does not have to perform a PCA, because the components are not correlated. That way is a little bit tricky because the numbers are no good quantities for the strength of correlation. The numbers are trends. Further, one cannot see nonlinear relations between components.

# Chapter 6

# Results

## 6.1 Probability of double and single pulses

The first result I am presenting here is the relative amount of double pulses to single pulses. This number is important to know, because I want to simulate these two groups separately. I will make a decision before the simulation, pulses from which group are to be simulated. Under the 18248 detected pulses there are 18007 single pulses and 241 double pulses. Concluding we have to simulate double pulses with a probability of 1.3 percent. In the other cases there will be a single pulse.

## 6.2 Single pulses

The fit process for single pulses delivers three numbers for each single pulse. Figures 6.1 to 6.3 show the distribution of the three-dimensional space projected on two axes.

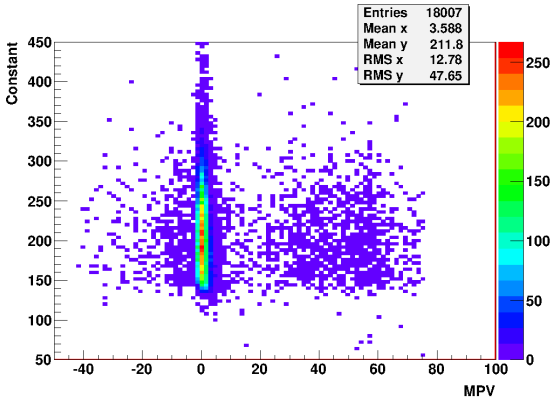


Figure 6.1: Distribution of Constant over MPV

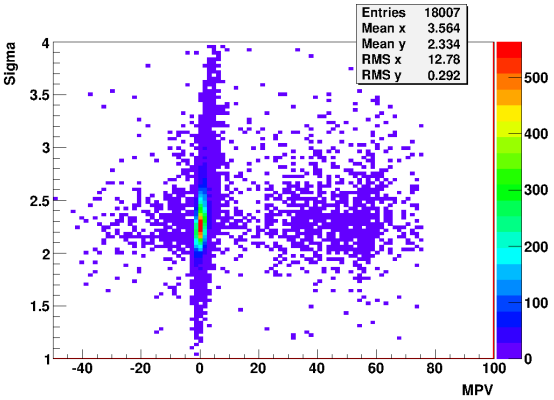


Figure 6.2: Distribution of Sigma over MPV

The first two figures show the distribution of the time-like parameter MPV to the other parameter axes. As one can see there are several areas. First most of the pulses are mainpulses where MPV is near zero. Left, next to them, there are pre-pulses. They are not shaped as an additional group, they are distributed in the negative time-range. On the right you can see the late-pulses as a wide cloud. This time-like distribution is interesting when one has in mind to characterize different pulses. Figure 6.4 shows this behavior in logarithmic scale. The maximum amount of main-pulses in one bin is two orders higher than that of late-pulses. Most late-pulses arrive at a time between 50 to 60 ns after the expected time for mainpulses.

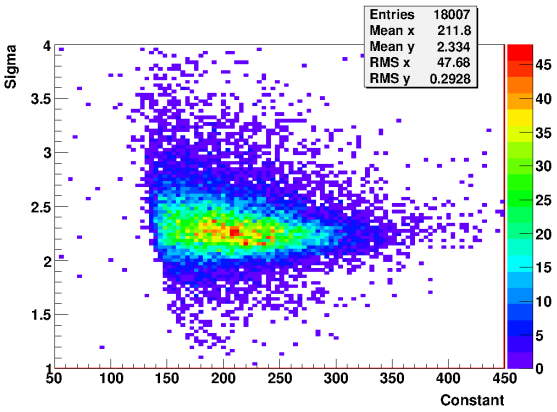


Figure 6.3: Distribution of Sigma over Constant

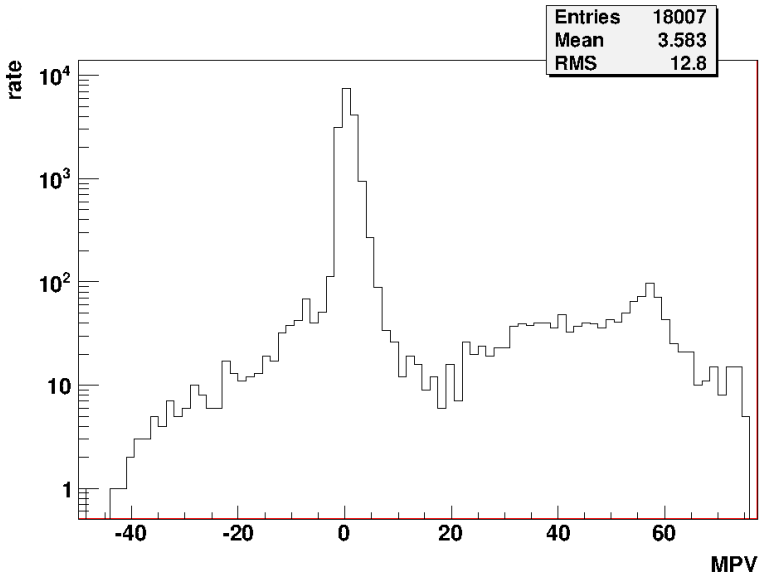


Figure 6.4: Distribution of MPV in single pulses

The following formula shows the normalized covariance matrix for each pair of parameters.

$$C = \begin{pmatrix} 0.3333 & -0.01417 & -0.04431 \\ -0.01417 & 0.3333 & 0.027 \\ -0.04431 & 0.027 & 0.3333 \end{pmatrix} \tag{6.1}$$

The columns and rows are filled with values in the arrangement constant, MPV and sigma. The message of this matrix is that there are only very small correlations, as seen in the histograms above. This is a first hint, that perhaps the PCA is not working so fine.
Figure 6.2 shows the sigma parameter. As one can recognize, there is a slight dependency in the data of the main-pulses. The covariances of the parameters shows exactly this behavior (see Equation 6.1). The corresponding value in line 3 and coulumn 2 is positive, e.g. the higher MPV the higher sigma is expected. But as one can see all values are very small. The other values of pre- and late-pulses also influence the matrix. Here a correlation cannot be seen directly, which makes it difficult to draw a definite conclusion.
Figure 6.3 shows the behavior between the Sigma and Constant. One can see that the higher the pulse is the smaller the width of pulse is.
What are the possibilities to receive simulated parameters?

**Simulation with 1D histograms** First we can use each distribution of the parameters to draw single parameters. The big advantage is that there is not much work to do and the storage needed is very low. There are only the values of non zero entries to be stored. In my case I used 100 bins for each histogram to get a satisfactory high resolution. The maximum storage I need are for 300 floating point numbers.
As one can imagine there is a big disadvantage, if there are high dependencies between the parameters. If one draws parameters out of the distributions projected to one dimension, you assume the parameters are independent. The dependency is not delivered by the single distributions.
Figure 6.5 shows simulated parameters out of one-dimensional distributions. One already sees that there is a loss of information. There is no slight decent in the main-pulses. The next figure presents the ratio between the original data to the simulated ones. The fact observed with the naked eye is confirmed. High values symbolize that there are less pulses simulated than in the original and the other way round.
In the other areas there is a agreement. Here one has to consider that in single bins deviations are to be neglected. They are evidences for the random process.

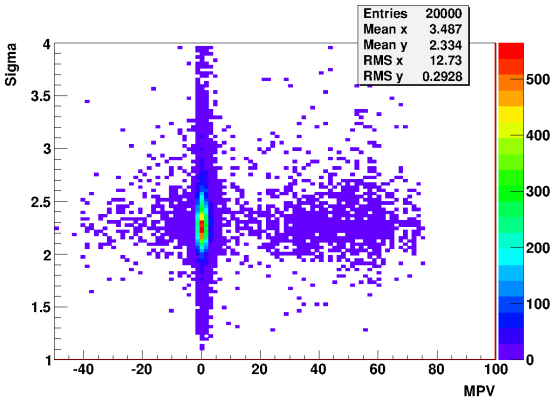


Figure 6.5: Distribution of Sigma over MPV simulated with 1D-distributions

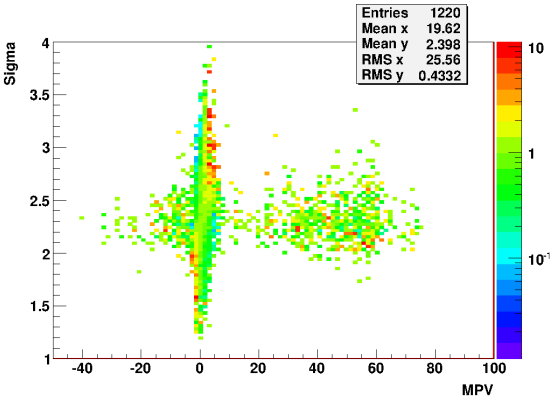


Figure 6.6: Distribution of MPV over Sigma, comparison between simulation and data

**Simulation with a 3D histogram** The next way one can handle the simulation process is to take the data and put it into a three-dimensional histogram. Finally you are able to draw random parameters out of these distribution. If there are in the same resolution as above, one can recognize that there is much data to store, even if I do only save non zero entries of the histogram.
Figure 6.7 shows the visualization of the parameters in a three-dimensional plot. The colors show the amount of pulses within a bin.
Finally I also tested the two-dimensional distributions out of this new simulation method for agreement to the original data. In the figures 6.8 to 6.11 one can see the related histograms.
The histogram of MPV and sigma shows the dependency lost in the method above. There is a slight correlation between the two parameters at the region of main-pulses. Next to the simulated distribution there is the diagram of the comparison. One can recognize that there is no deviation, other than in the last method. In the middle parts of the clouds it seems to be a better simulation than on the outer parts. This is a effect of the range of numbers. In the outer regions there are only spots with a little number of pulses so if there are one more or less

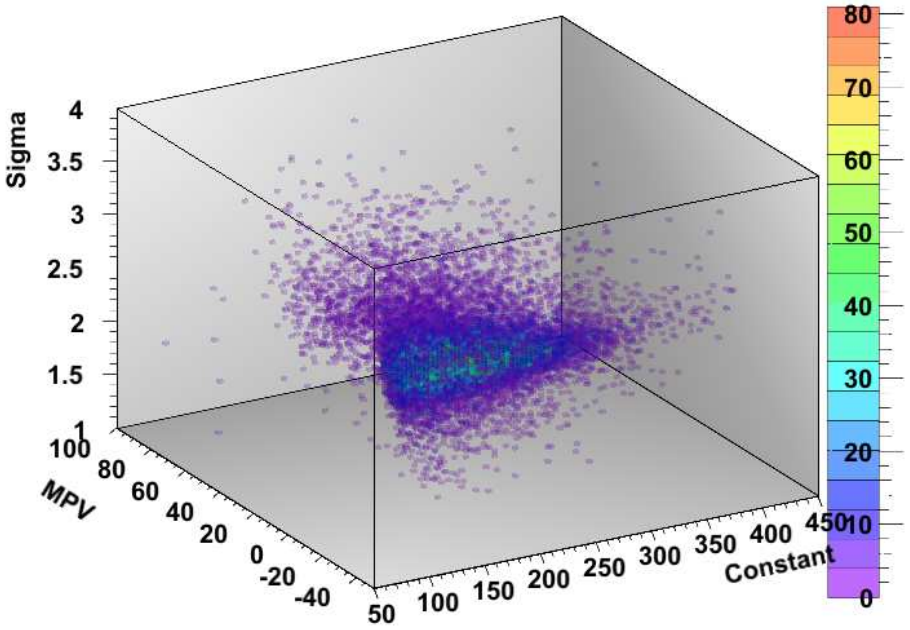


Figure 6.7: Visualization of the single pulse parameters

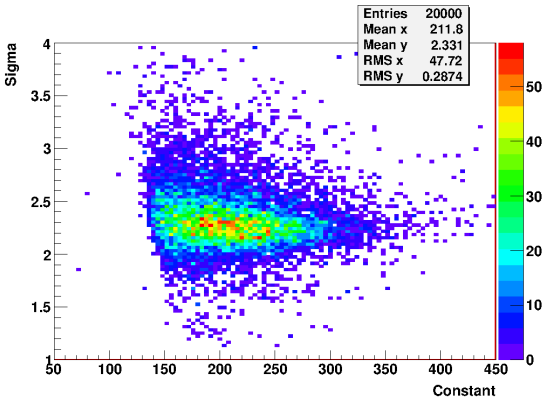


Figure 6.8: Distribution of Sigma over Constant simulated with 3D-Histograms

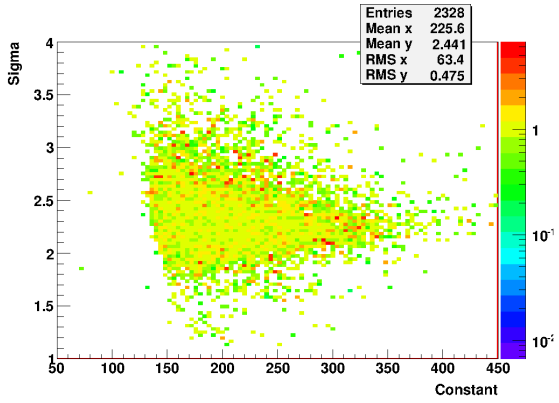


Figure 6.9: Distribution of Sigma over Constant simulated with 3D-Histograms, comparison between data and simulation

in the simulation, there is a big deviation. It is important, that the distribution of numbers smaller and bigger than one is approximately equal in all regions.

**Simulation PCA** The third way to simulate the parameters involves the principal component analyses. First the PCA has to be performed. The main outcome are two functions to transform parameters from the pattern space to the feature space and the other way round.
The first step is to generate histograms out of the data transformed to the feature space. Out of these histograms one can draw new random parameters, which are to be transformed back to the pattern space.
In the first step I already saw that the PCA does not work well in this case. One sees that there are dependencies in the parameters of feature space. (see figures 6.12 and 6.13). What could the problems be? First there are very spare data distributed over a wide range.

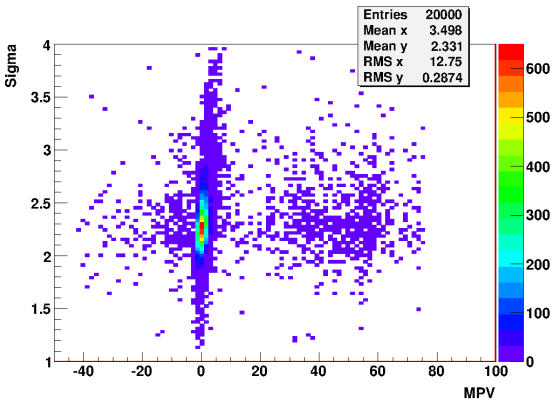


Figure 6.10: Distribution of Sigma over MPV simulated with 3D-Histograms

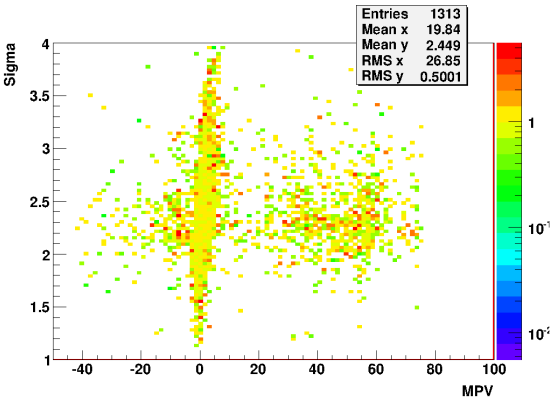


Figure 6.11: Distribution of Sigma over MPV simulated with 3D-Histograms, comparison between data and simulation

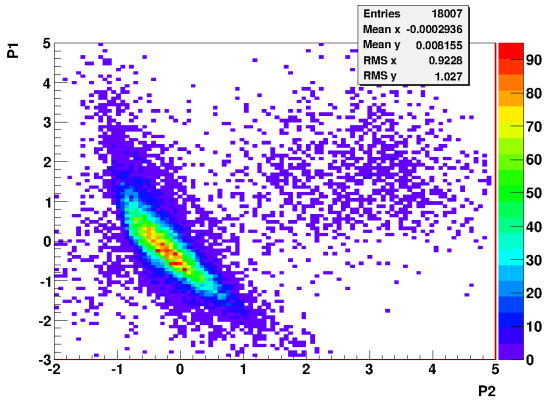


Figure 6.12: Distribution of P1 over P2 of PCA

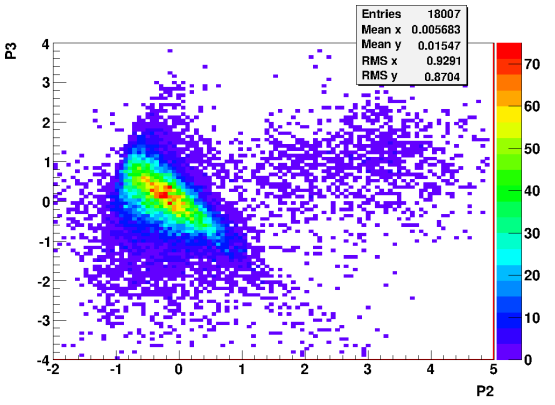


Figure 6.13: Distribution of P3 over P2 of PCA

As one can imagine, with this data there is no way to simulate new pulse parameters in a proper way. There is no agreement in the data simulated and measured data.
The final result of single pulses is that I am going to simulate new parameters by the three dimensional histogram. 6945 bins are of a non zero value. If the performance has to be higher one can change to the original one dimensional histograms, but be aware of the loss information.

## 6.3 Double Pulses

Double pulses are described with six instead of only three parameters. Due to that, the easiest way to draw new random parameters is not to take a histogram of the necessary dimensionality, because ROOT delivers no six dimensional histogram. Further on this would lead to a very high amount of data to store of $N^6$ with N being the bins per dimension.
Additional to the search of a non trivial drawing method, there is a quite hard problem, I cannot get rid of in this bachelor thesis. In the used data there were only 241 double pulses. This is a very low number in sense of statistics. But the following considerations are universal for more data. The comparing plots as seen in the last chapter about single pulses cannot be used here. If in one of the comparing histogram the bin content is zero there is no data in the created histogram. Concluding there is even fewer entries than in the underlying histograms.

Following one can read the covariance matrix delivered by the ROOT-PCA routine TPrincipal. The parameters are numbered as in the chapter above. Additionally the three parameters of the second pulse are attached in the same order.

$$C = \begin{pmatrix} 0.1667 & -0.02605 & -0.0137 & -0.0233 & 0.01824 & -0.02992 \\ -0.02605 & 0.1667 & 0.00202 & -0.01179 & 0.09853 & 0.017 \\ -0.0137 & 0.00202 & 0.1667 & -0.00512 & 0.005017 & 0.01737 \\ -0.0233 & -0.01179 & -0.00512 & 0.1667 & -0.0006312 & -0.0271 \\ 0.01824 & 0.09853 & 0.005017 & -0.0006312 & 0.1667 & -0.003842 \\ -0.02992 & 0.017 & 0.01737 & -0.0271 & -0.003842 & 0.1667 \end{pmatrix} \tag{6.2}$$

As one can see there are only small values standing for less correlations between the parameters. In the element of the MPV of the first pulse and the MPV of the secound pulse are indizes which could stand for a correlation with a higher impact. The definition of first and second pulses leads to different time distributions, causes different distributions in the MPV. In fact there cannot be some second pulses before the first pulse. Figure 6.14 shows the corresponding histogram. Here also one can see the agglomeration of main-pulses with after-pulses in MPV regions of 20 to 80.

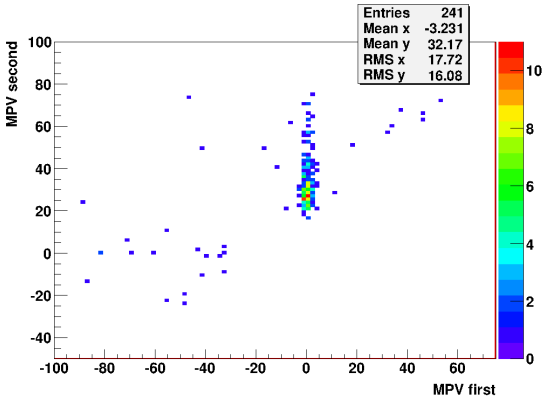


Figure 6.14: Distribution of MPV 2 over MPV 1 of original data

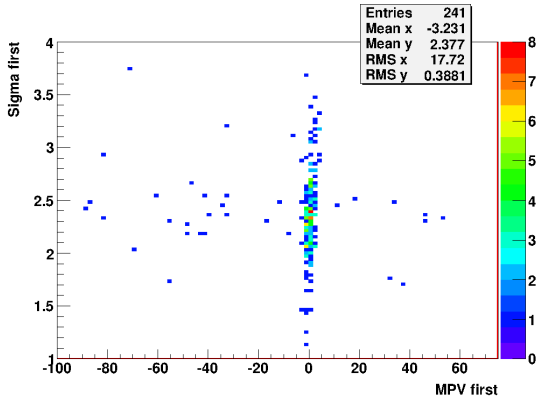


Figure 6.15: Distribution of Sigma 1 over MPV 1 of original data

Figure 6.15 shows the behavior of the MPV to the sigma value of the first pulse. As in the last chapter we see there is a slight dependency between these two parameters. The corresponding parameters of the second pulse are shown in figure 6.16. Because there is not such a big agglomeration of pulses in one region of MPV one cannot detect a correlation in that case.
One more example for the distributions projected into two dimensions are shown in figures 6.16. That example is typical for the other distributions. One cannot see directly any correlations. Out of the two-dimensional distributions one can see there are three parameters which depend on each other.

**Simulation with 1D-histograms** The first attempt to simulate new parameters is drawing the numbers out of one dimensional distributions. Because in the comparing plots there have too few entries I do not show them here. They do not transport much information.
The simulated sigma and constant of the first pulse is shown in figure 6.18. The distribution is quite similar to the original data. That is also true for most of the other distributions.
Figure 6.19 shows the distribution of the time-like axes. You can see there are double pulses with the second before the first. So using uncorrelated parameters simulation in this case is not an acceptable way to receive simulated pulses.

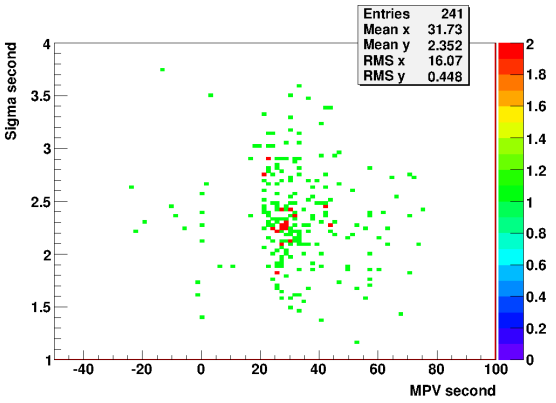


Figure 6.16: Distribution of Sigma 2 over MPV 2 of original data

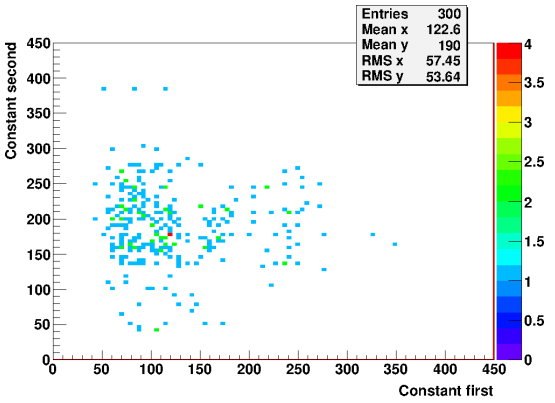


Figure 6.17: Distribution of MPV 2 over MPV1 simulated with 1D-histograms

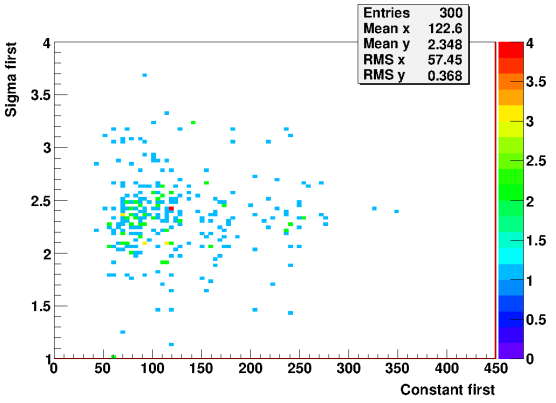


Figure 6.18: Distribution of Sigma 1 over Constant 1 simulated with 1D-distributions

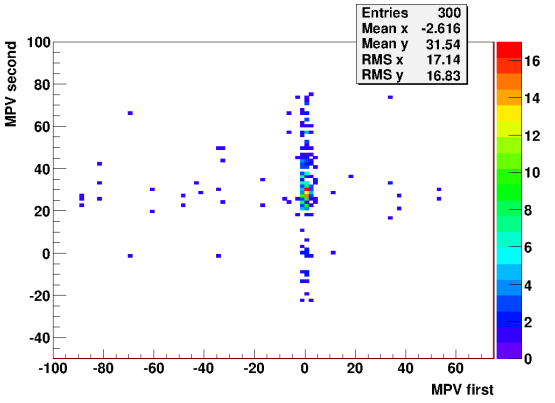


Figure 6.19: Distribution of MPV 2 over MPV 1 simulated with 1D-distributions

**Simulation with PCA** The second way to generate pulses is to perform a PCA on the measured data, using the histograms of transformed data to draw new parameters for pulses. One can assume that because the parameters are distributed in an homogeneous shape in most cases, the PCA should work well.

A few first figures are shown from figure 6.20 to 6.23. All histograms have one similarity. The entries are more distributed over the space than the original data. The first figure is the best, the distribution looks nearly the same as the original.

Figure 6.21 shows the most drastic result. In the simulation there is a widely distributed cloud of pulses. The original histogram has a thin line around an MPV of zero. The result in simulation would be that there is a bigger variance in the time of the pulses. The next figure shows histograms with the distribution of the timelike axis and a sigma value. Again the time is smeared.

The final figure of this series shows a good example of PCA modeling. If one compares it to the original, one can see the fit is very good. There are a few entries around zero and the most entries are around 40 in a wide cloud.

We see the PCA works well if there are parameters localized in a cloud with some spread. The method does not work well if there is a very agglomerative line and some other spread parts around. The PCA tends to smear out the data over the whole parameter range.

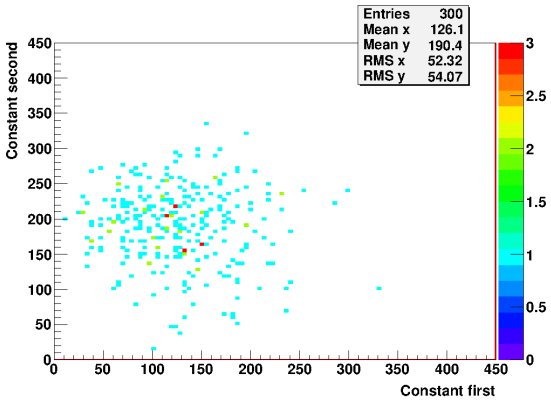


Figure 6.20: Distribution of Constant 1 over Constant 1 simulated with PCA

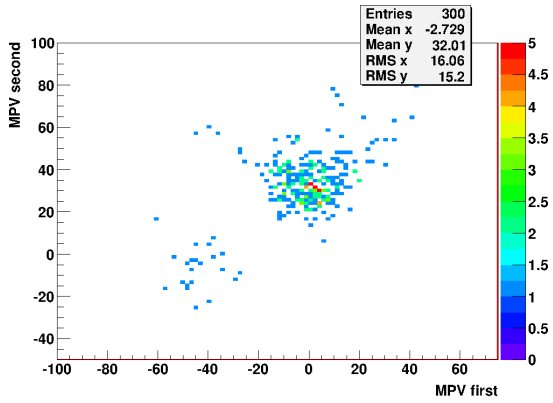


Figure 6.21: Distribution of MPV 2 over MPV 1 simulated with PCA

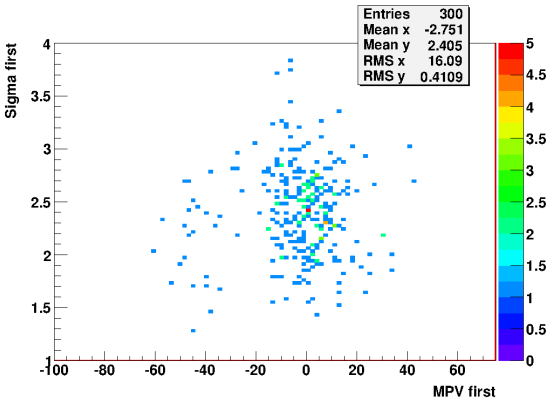


Figure 6.22: Distribution of Sigma 1 over MPV 1 simulated with PCA

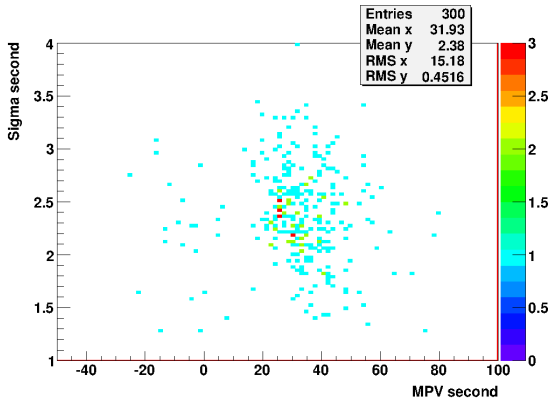


Figure 6.23: Distribution of Sigma 2 over MPV 2 simulated with PCA

**Simulation with combination of 3D and 1D histograms** The final method I tried to generate new random pulses is to combine the method I used for single pulses with the well working method of original 3D histograms and the remaining dimensions are simulated by one dimensional histograms.

As one saw in the original histograms, the main dependencies between the parameters lie in the timelike axes MPV and between the MPV and sigma of the first pulse. One can put these three parameters into one histogram of three dimensions. The remaining parameters are drawn out of 1D histograms. If there are more closed circles of dependencies, one can make more such higher dimensional histograms. Here it is not necessary.

Figures 6.24 to 6.27 show the result of this methode. The results are mostly very similar to the original data. As expected, the right order of first and second pulse is achieved.

As seen in the last chapter, the method of three dimensional data aquisition is the best way.

In the upper region of the figure 6.24 one sees one problem, which one always has with distributions generated with one dimensional distributions. There can be straight lines due to one entry in the histogram. The distribution of the other dimension leads to a smearing effect over the whole histogram arranged in a line, even if there is no measured pulses in the underlying data at this bin.

The final message for this method is that we combined the storage saving method of one dimensional histograms with the method of the best accuracy, the storage of three dimensional

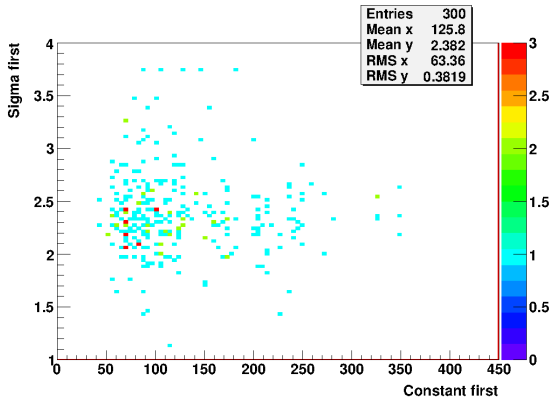


Figure 6.24: Distribution of Sigma 1 over Constant 1 simulated with combined method

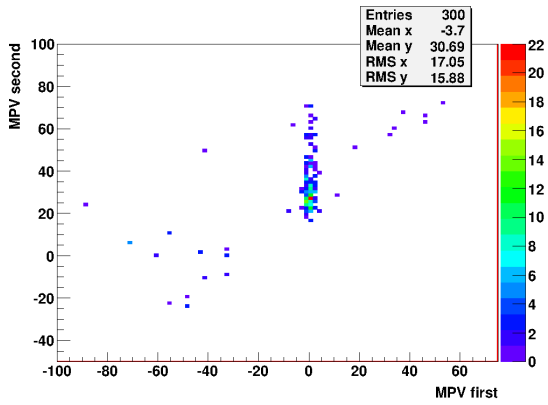


Figure 6.25: Distribution of MPV 2 over MPV 1 simulated with combined method

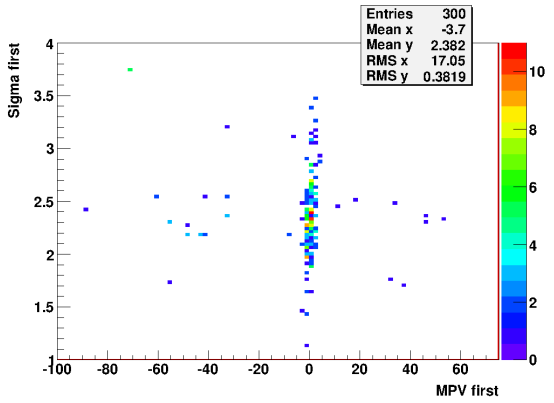


Figure 6.26: Distribution of Sigma 1 over MPV 1 simulated with combined method

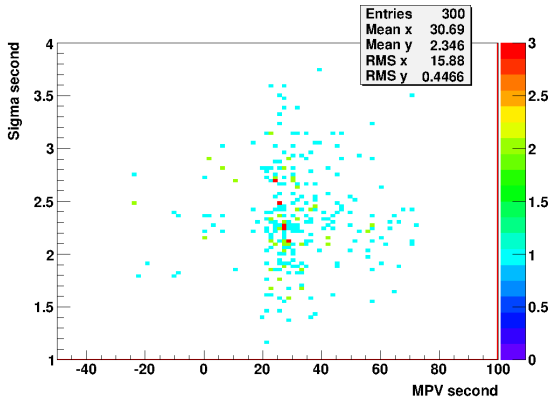


Figure 6.27: Distribution of Sigma 2 over MPV 2 simulated with combined method

information. For more precision one needs more data of double pulses. In the shown histograms there are only 241 measured pulses the simulated number is 300. In the special case of comparing histograms in terms of getting the ratio between them, one needs closed data clouds. Closed data clouds are distributions with entries in each bin.
One can try to reduce the resolution of the histogram. As seen in the considerations, if there are dependencies in the parameters, they are very small. In the used resolution they are only up to the size of ten bins. So if one increase the bin size the dependencies could vanish.

## 6.4 Pulse charge

Finally I will test if the simulation reconstruct the same charge distribution as the original pulses. This is also of interest for the energy reconstruction of the muons.
The charge can be measured by the integral of the pulses. Commonly one sets the integral value with the highest amount of entries to a charge of one single electron, as one thinks all pulses are created by single photons. As the response of a photomultiplier is linear, the transformation of the axis of charge is just a multiplication.
Figures 6.28 shows the charge distribution of pulses of the original data. The mean value is 484.6 and the root mean square is 114.4. There is a maximum at around 440. Here I say the

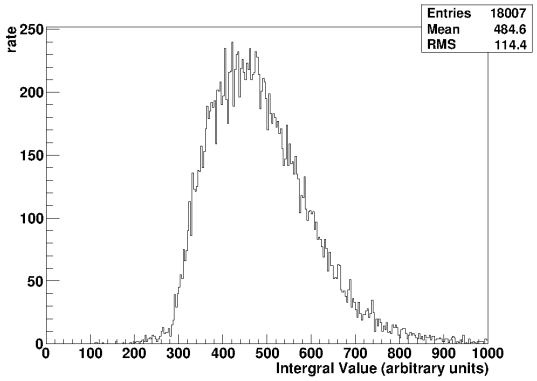


Figure 6.28: Charge distribution of data single pulses

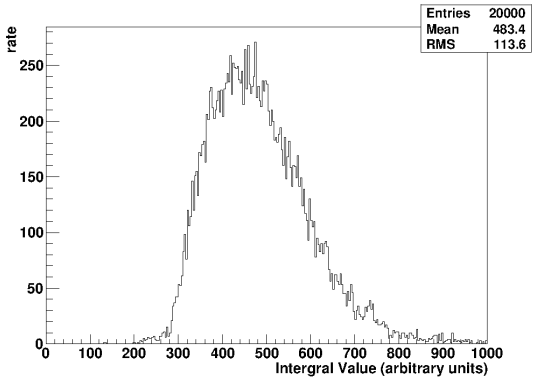


Figure 6.29: Charge distribution of simulated single pulses

pulse has a charge of one photoelectron. I do not take the absolute maximum of values in the histogram lying at 420. I fit a polynom of degree 6 to the range from 300 to 600 and receive a the described maximum.
The shape is formed by big amount of entries around the mean value. On the lower side there is a steeper rise than on the upper side.
The distribution for the simulated pulses is shown in figure 6.29. The mean value is equivalent to the mean of the original data, with a precision lower than 0.25 %. The agreement of the root mean square is up to 1 %.

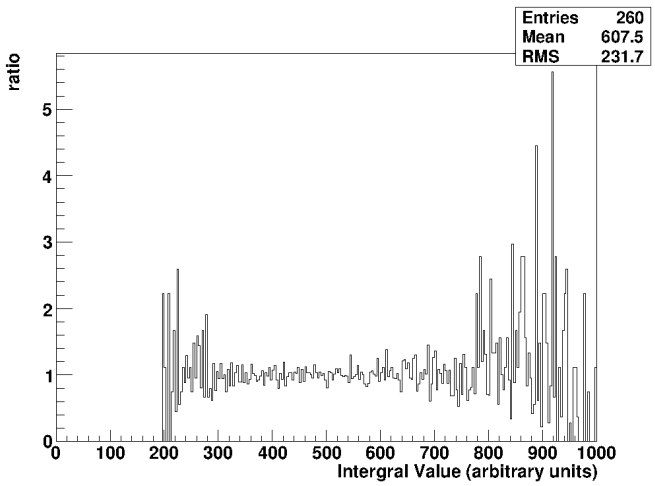


Figure 6.30: Comparison between charge of data and simulation of single pulses

To illustrate the agreement between the simulation and the data figure 6.30 shows the quotient of the two histograms above. Over a wide range from 300 to 800 one can see a value nearby one, standing for good agreement. In the outer ranges there are some deviations between the to histograms, caused by the low number of entries.
The same test is made for the double pulses. The shape is similiar to the single pulses. There is a steep rise at the lower edge and a longer tail at the upper regime. The mean value for the pulses out of the data is 361.7. It is smaller than the value of single pulses, because the charge has to be deployed in two pulses. But the value is not the half, as one could assume at first glance. Out of the values one recognizes the complete charge of a double pulse is higher than

of a single pulse.
Again there is a high agreement between simulated pulses to measured pulses. The mean deviates only by less than 2%. The higher value than seen for single pulses are caused by the low number of entries.

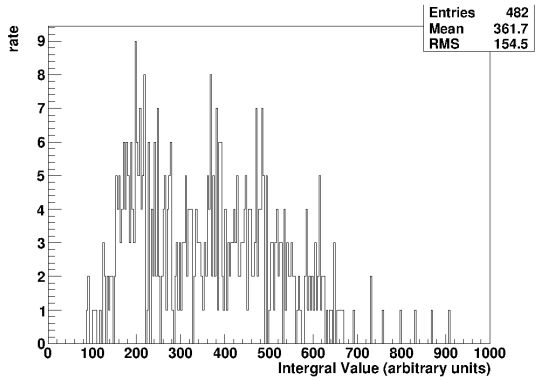


Figure 6.31: Charge distribution of data double pulses

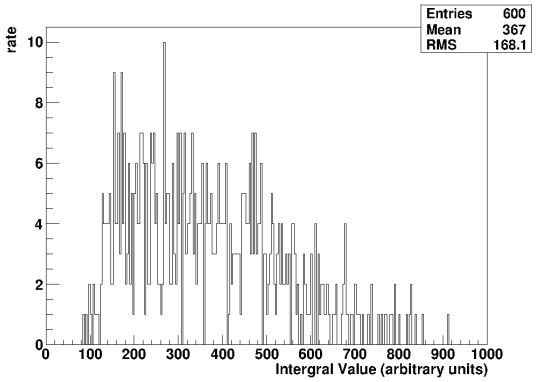


Figure 6.32: Charge distribution of simulated double pulses

In figure 6.33 there is the comparison of the two histograms above. There is a tendency for values nearby one. But one can see some deviations as expected.

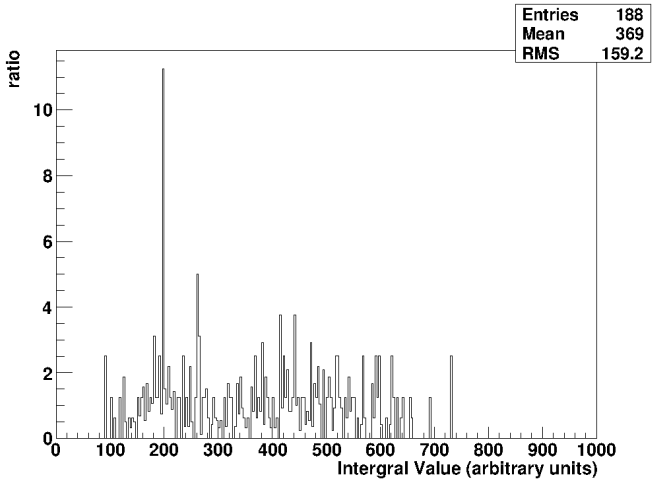


Figure 6.33: Comparison between charge data and simulation of double pulses

Concluding this last test before the application in Seatray is satisfying. The simulated pulses have similar properties to the original pulses.

# Chapter 7

# Application in SeaTray

This last chapter aims to introduce the application of the simulation to the SeaTray framework described in the first part. The different approaches to a simulation of minimum bias events are compared to actual data.

## 7.1 Introduction to Seatray

Seatray is a framework-based analyses toolkit for ANTARES. It has a modular structure to be easyly used by the end-user. The end-user is to be able to use separate modules, arrange them in a working chain and change some input parameters to solve a problem.
Due to the fact that the framework is modularized, all modules shall work independently of each other. This leads to a user friendly interface.
The modules build up an analysis chain. Through that chain one can push so-called frames. Frames are unites of information, like the current detector geometry, calibration or the information about Cherenkov light reached the photomultipliers. Each frame is passed through the chain of modules.
Seatray is able to handle raw and Monte Carlo data. Seatray is used for data processing as well as for simulation processes as I do in this bachelor thesis.[7]

## 7.2 Processing chains in Seatray

In the following section I will test the new method against the existing modules.
There are several modules to simulate the Optical Module. Figure 7.1 shows the different approaches. All chains begin with a file of data. Even if I do not use the data of hits in it, the simulation needs an OM-Condition map. This maps contains the current information of the functionality of the Optical Modules and the photon countrates per OM.
On the left one sees the chains of SeaTray. It starts with the I3NoiseHitsAdder. This module generates 1 p.e. hits. These hits are passed to the next module. The old SeaTray module I3AntPMTTTSSimulator simulates the response of the photomultiplier. The output of this module are so-called recopulses, which already give an integrated charge and time smeared to the measured timing distribution of the PMT. The ARS-Simulator afterwards adds up complete recopulses which arrive within an integration window of an ARS. Because there is a assumption of ideal pulses and there is no step, which involves the actuel influence of deviating PMT behaviour in the various OM, one has to smear the charge and the time within the PMT simulation. The chain continues with the de- and recalibration,
In contrast there is the new method of waveform simulation. One has to use the I3AntPMT-WaveformSimulator. Here whole waveforms are generated as described above. These waveforms

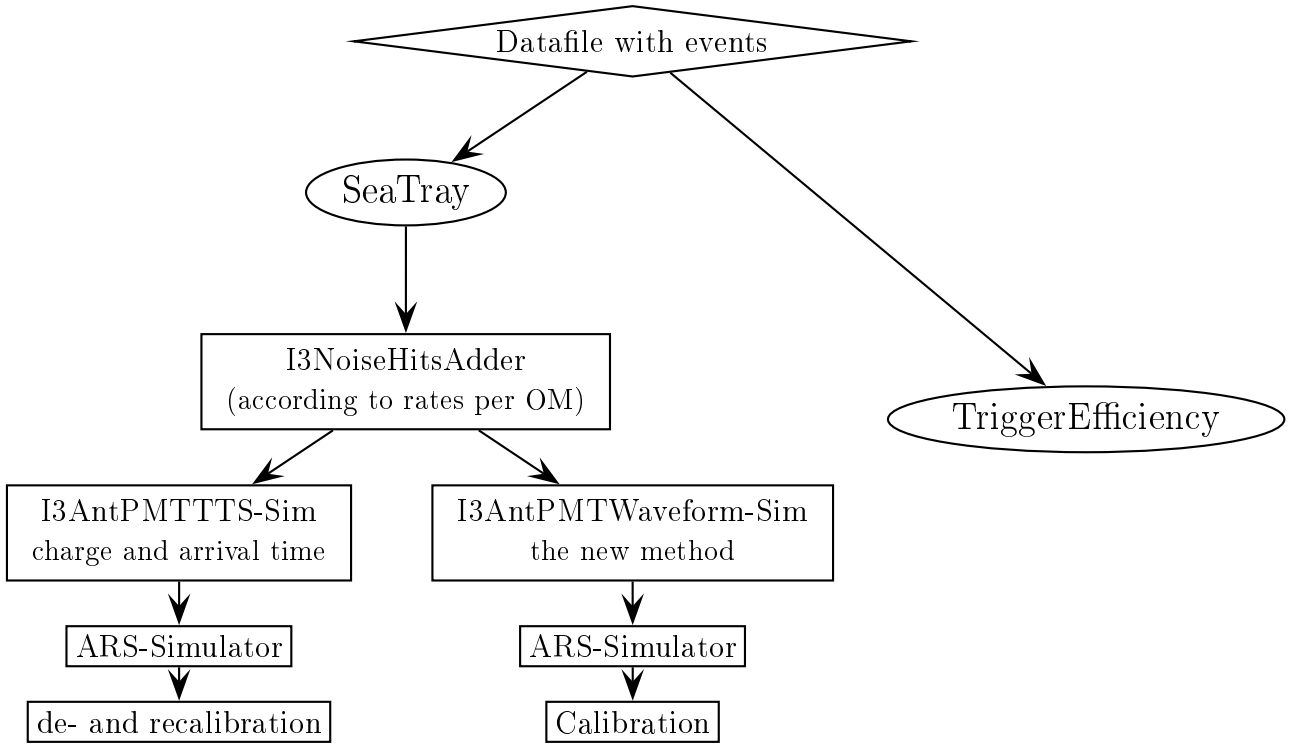


Figure 7.1: Possible chains of simulation

are passed to the new ARS-Simulator, which is able to receive the AVC and TVC, charge and time equivalents, out of the waveforms by integration processes. The output is the raw-data format of ANTARES, so-called AntSPE-Hits. Finally there is the calibration, which generates calibrated recopulses with a charge and time from the SPE-Hit. Here more work has to be done to simulate the calibration process in ANTARES to receive an even better result than until now.
On the right there is TriggerEfficiency a standalone analyses toolkit.
For the tests above I have used Minimum Bias data out of the run 49995 and 52965 out of the year 2010.

## 7.3 Results of comparison

It is good to know how the implementation is working to understand the results I am presenting in this chapter. The key facts ANTARES is interested in are the charge of pulses and the time of arrival. So I will concentrate my analyses to this points.

**Charge distribution of pulses** First I will have a look at the charge distribution of pulses. Figures 7.2 and 7.4 show the distributions of the charge in the pulses detected. One detail is obvious. The charge of Minimum Bias hits are more spread around the mean value near 1 p.e. There are some calibration processes in the ARS, which are not simulated in the current version so well. It can be reduced to that we are assuming too ideal pulses coming out of the PMT than it is in reality. The result would be that the charges are spread over a wider range. Even without this step the resulting values representing the measured data very well.
In fact I used here a generic way to simulate the pulses. In contrast the other simulations uses distributions for the charge and time of arrival and simulate charge smearing from the observed distribution in data.

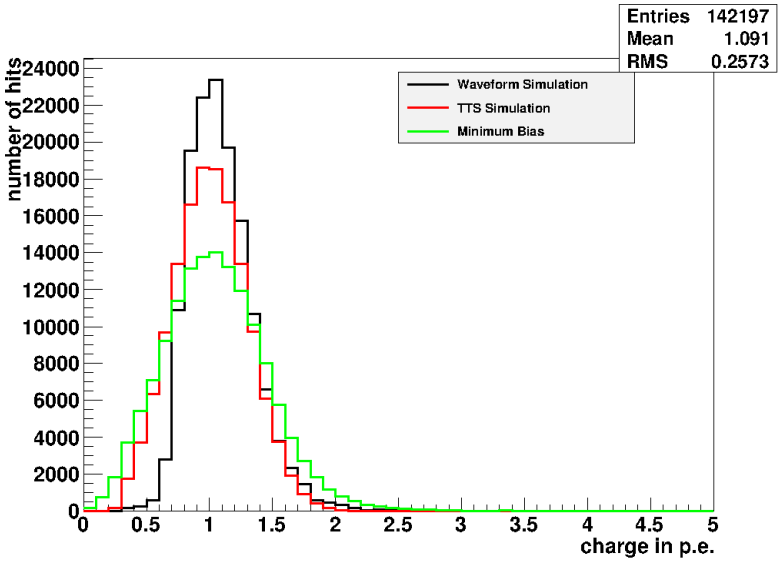


Figure 7.2: Charge distribution of pulses of different simulation methods by run 52965

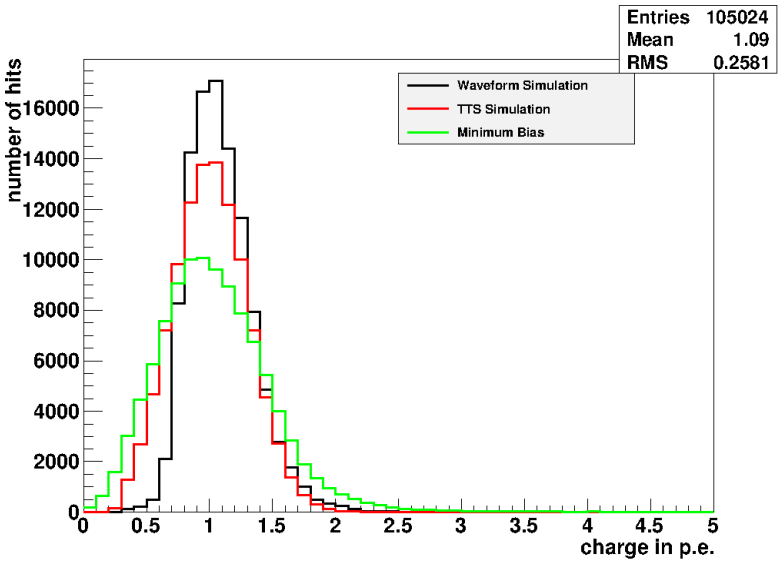


Figure 7.3: Charge distribution of pulses of different simulation methods by run 49995

In Figure 7.3 one sees another example of a simulation. That is not only an other simulation with the same OM condition map, but I use the different run 49995. The main facts of the distributions are the same. The shown examples are no arbitrary results, but reproducible for different runs.
The charge distribution of a simulation with TriggerEfficiency is shown in figure 7.4 with the distribution of Minimum Bias hits. We see the distribution fits quite well.
Finally one sees the Waveform Simulation leads to a similar to the real distribution.

**Charge distribution of after-pulses** Further I compare the charge distributions of after-pulses, which can be distinguished by being a second hit after a prior photon detection on the same OM.

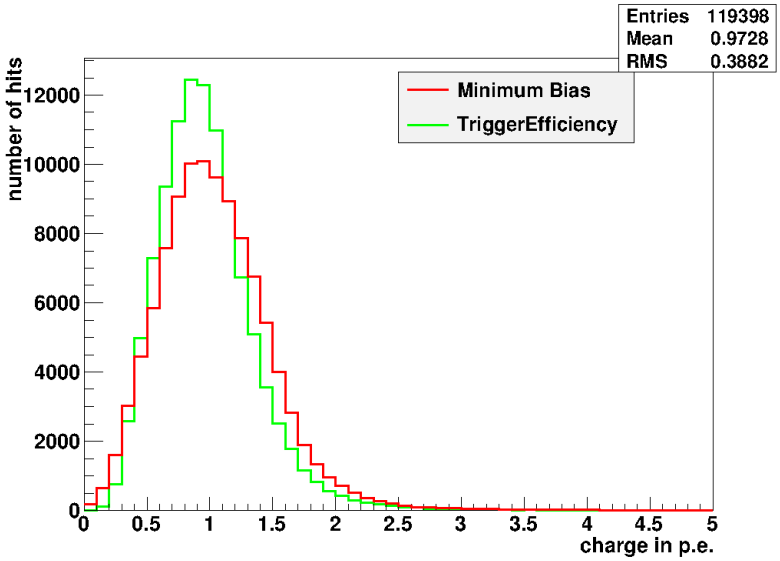


Figure 7.4: Charge distribution of pulses of different simulation methods by run 49995

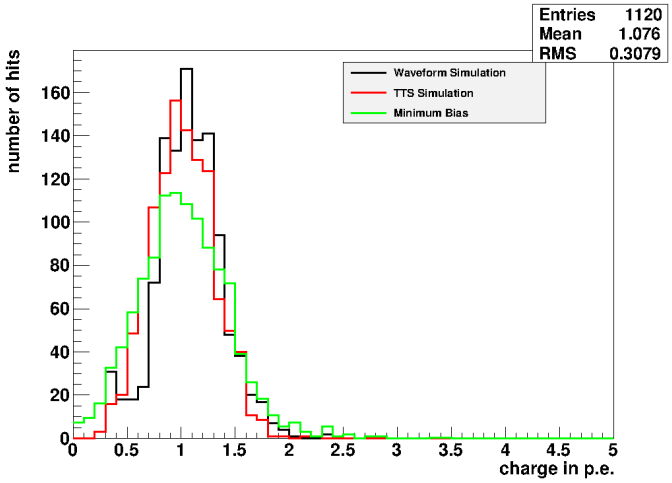


Figure 7.5: Charge distribution of after-pulse of different simulation methods

Figure 7.5 shows the charge distribution of after-pulses. One sees a distribution around 1 p.e. as expected. There is a peak at 0.3 p.e. due to the integration in the ARS module. This is no effect of this single simulation, this effect is seen in other simulations with the Waveform Simulator, too. Adapting the waveform simulation to less ideal PMT conditions might result in smearing out this peak at 0.3 p.e. and thus contribute to the observed charge distribution.

Concluding there is a higher agglomeration around the mean value in the new simulation than in the Minimum Bias data.

Figure 7.6 shows the distribution resulting from TriggerEfficiency. Here one can see the biggest agreement to the Minimum Bias data. Also here a tendency of a to narrow distribution is recognizable.

The final two plots show the charge distribution of the second pulse over the first pulse. The problems in both groups of pulses are recognizable. The distribution is to wide due to the assumption of too ideal pulses leaving the PMT.

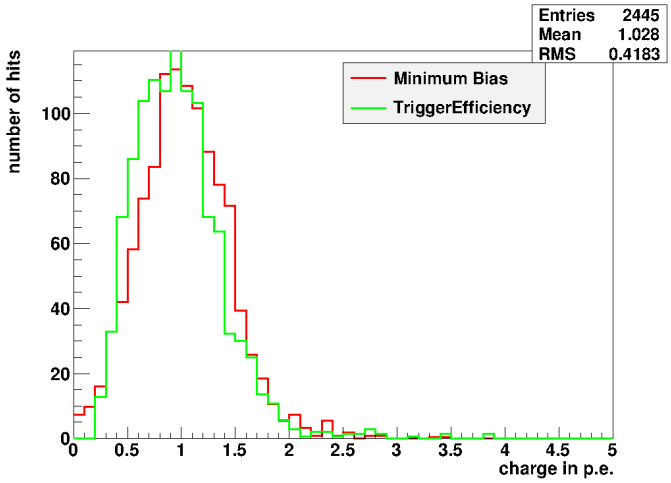


Figure 7.6: Charge distribution of after-pulses of different simulation methods

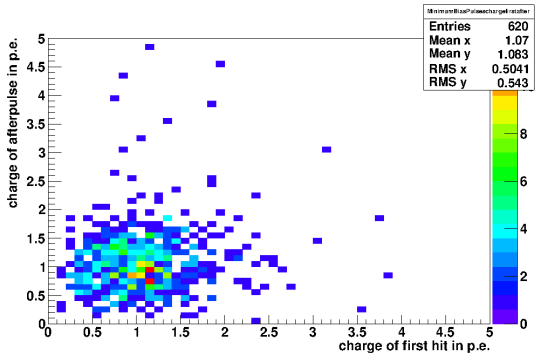


Figure 7.7: Charge distribution of pulses of Minimum Bias events

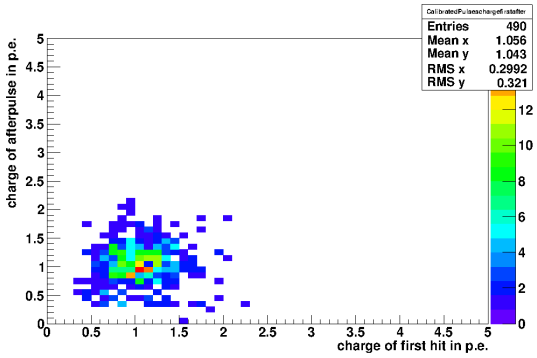


Figure 7.8: Charge distribution of pulses simulated with Waveform-Simulation

**Arrival time difference for consecutive hits** The next comparison will concern the time of arrival. Figures 7.9 to 7.12 show the distribution of arrival time of hits with respect to the

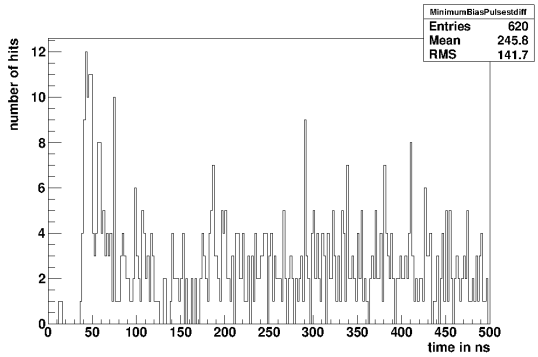


Figure 7.9: Arrival time difference for consecutive hits in Minimum Bias Events

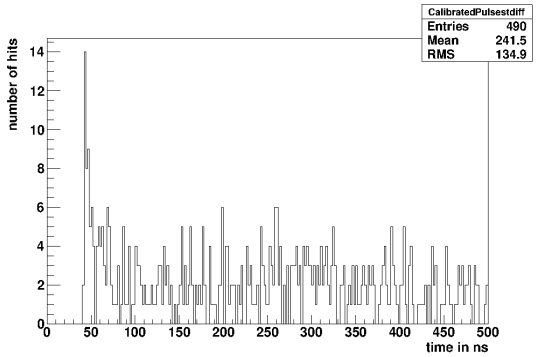


Figure 7.10: Arrival time difference for consecutive hits simulated with waveforms

previous one. One can recognize that there is an empty region up to around 40 ns due to the dead time of the ARS. In the time directly following there are to be more pulses than in the rest of the time axis as shown in the plot with Minimum Bias events. This excess is caused by afterpulses, which occure in the first 80 ns seconds as mentioned in the chapter about the Optical Module. TriggerEfficency and the Waveform Simulation both show this effect.

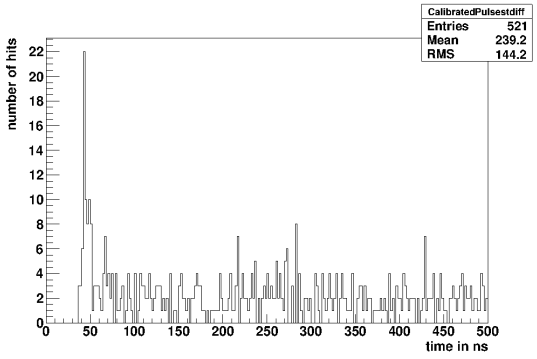


Figure 7.11: Arrival time difference for consecutive hits simulated with TriggerEfficency

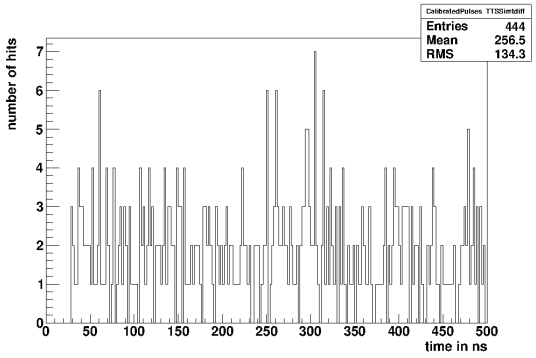


Figure 7.12: Arrival time difference for consecutive hits simulated with TTSSim

I show here the ratio between the rate in the first excess region up to 80 ns to the baseline region to receive a qualitative feedback how good the simulations are. The ratio is called R in the following. For the ratio I counted all hits up to 80 ns and calculate a value for the rate by dividing by the time from the first counted hits to 80 ns. In analogue I count the hits in the rest of time. The results are shown in the table 7.1.

Table 7.1: Rate ratio R of excess to basline

| | Minimum Bias | WaveformSimulation | TriggerEfficency | TTSSim |
|---|---|---|---|---|
| $R_{49995}$ | 2.36 | 2.26 | 2.56 | 1.06 |
| $R_{52965}$ | 2.40 | 1.76 | 2.02 | 0.81 |
| $R_{53003}$ | 1.79 | 1.31 | 1.52 | 0.82 |

The numbers of each line refer to a simulation based on one specific run.
The results say that in the first 40 ns of measured hits there are R-times more hits than in the baseline. TriggerEfficency is in this example very close to the Minimum Bias data. The Waveform Simulation leads also to an good value in term of a maximal deviation of only maximal 10% in this examples. The look to all simulations leads to the conclusion that the Waveform Simulation to the Minimum Bias values. than the other values.
If one has a closer look to the diagrams, one can recognize differences in time of start. That means the Minimum Bias events start at a time of 36 ns, the TriggerEfficency, too. The new method, WaveformSimulation is starting at 40 ns. That can be corrected by the right choice of some parameters in the SeaTray module. The TTS-Simulation starts even earlier, indeed in this simulation is more offset than in the other ones.

# Chapter 8

# Conclusion and outlook

This bachelor thesis is about the simulation of the response of the Optical Modules in the ANTARES neutrino telescope. The simulation is based on data taken from a setup similar to that used in ANTARES. These pulses are analyzed and reduced to characteristic numbers. Finally I had to think about the correlations of the parameters and the possible effect on a simulation.
In the used data only small effects of correlations are observed. The attempt to fight it with a Principal Component Analyze failed or did not bring a big advantage so I took the method to draw new parameters out of a high-dimensional histogram or combined with additional one-dimensional histograms. In this way all correlations of the parameters are fulfilled.
The analyses were completed with some comparisons between original distributions and simulated distributions.
The analyses led to different simulation methods for single and double pulses. Single pulses are to be simulated by a three dimensional histogram. All correlations of the original data are preserved and one receives a very precise reconstruction. Double pulses are simulated by a combination of methods. First I looked for the most correlated parameters. They are simulated by a three-dimensional histogram. The remaining parameters are simulated by one-dimensional distributions out of the original data.
The final test for agreement were the charge distributions. Here I could see the simulated charges fit very well to the measured data.
One remark concerns the number of pulses used for the analyses. As one sees in the figures about double pulses, there are very spare data. It is desirable to get data covering the whole parameter space.
In the last chapter one can see the application of the simulation in the SeaTray-Framework. The simulation delivers very good results, one receives a distributed charge similar to the distribution received from Minimum Bias events. The Minimum Bias data are spread over a bigger range. This discrepancy is caused in calibration process, where pulses are smeared. This calls for more exact modeling of PMT parameters, like the gain.
After-pulses type 2 were not treated here, because of the lack of data. That would be a next step to improve simulations.
Finally it would be necessary to simulate not only pulses around the charge of one photo electron, but also other charges. Therefore one needs data out of such experiments. The simulation steps after is the same as described in this bachelor thesis.
Afterwards are there is a new generic way to simulate the response of the Optical Modules, in contrast to the old simulations with some distributions in it, which can be used to enhance the understanding of PMT behaviour within the ANTARES detector.

# Bibliography


[1] G. Bourier. *Wahrscheinlichkeitsrechnung und schliessende Statistik*. Gabler, 2011.

[2] T. Chiarusi and M. Spurio. High-energy astrophysics with neutrino telescopes. *The European Physical Journal C - Particles and Fields*, 65:649–701, 2010.

[3] ANTARES Collaboration. The antares optical module. *Nuclear Instruments and Methods in Physics Research Section A: Accelerators, Spectrometers, Detectors and Associated Equipment*, 484(1-3):369 – 383, 2002.

[4] ANTARES Collaboration. Transmission of light in deep sea water at the site of the antares neutrino telescope. *Astroparticle Physics*, 23(1):131 – 155, 2005.

[5] ANTARES Collaboration. Performance of the front-end electronics of the antares neutrino telescope. *Nuclear Instruments and Methods in Physics Research Section A: Accelerators, Spectrometers, Detectors and Associated Equipment*, 622(1):59 – 73, 2010.

[6] ANTARES Collaboration. Search for cosmic neutrino point sources with four years of data from the ANTARES telescope. *arXiv:1207.3105*, July 2012.

[7] T. Eberl and C. Kopper. The seatray software framework. *ANTARES-SOFT-2009-013*, May 2009.

[8] L. Gauchet and A. Creusot. Black box set-up and first results on the antares optical module. *ANTARES-OPMO-2012-001*, Jun 2012.

[9] J. P. Gómez-González and for the ANTARES Collaboration. Calibration systems of the ANTARES neutrino telescope. *arXiv:1204.5021*, April 2012.

[10] J. D. Jackson. *Klassische Elektrodynamik*. de Gruyter, Berlin/New York, 3 edition, 2002.

[11] U. F. Katz and C. Spiering. High-energy neutrino astrophysics: Status and perspectives. *arXiv:1111.0507*, November 2011.

[12] Hamamatsu Photonics K.K. *PHOTOMULTIPLIER TUBES Basics and Applications*. Hamamatsu Photonics K.K., 3. edition, 2006.

[13] K. S. Koelbig and B. Schorr. A program package for the landau distribution. *Comput. Phys. Commun.*, 31(CERN-DD-83-18):97–111. 21 p, Jun 1983. Erratum published in 2008: Comput. Phys. Commun. 178 (2008) 972.

[14] V Kulikovskiy, M Anghinolfi, K Gracheva, M Taiuti, and Y Yakovenko. The measurement of late-pulses and after-pulses in the large area Hamamatsu R7081-20 photomultiplier used in the ANTARES telescope. May 2011. ANTARES-OPMO-2011-002.

[15] L. Landau. On the energy loss of fast particles by ionization. *J. Phys. (USSR)*, 8:201ff, 1944.

[16] M. Loeffler-Mang. *Optische Sensorik: Lasertechnik, Experimente, Light Barriers*. Vieweg+Teubner Verlag, 2012 edition, December 2011.

[17] K. Nakamura and Particle Data Group. Review of particle physics. *Journal of Physics G: Nuclear and Particle Physics*, 37(7A):075021, July 2010.

[18] B. Povh, K. Rith, C. Scholz, and F. Zetsche. *Teilchen und Kerne: Eine Einfuehrung in die physikalischen Konzepte*. Springer, 8. edition, March 2009.

[19] A. Schukraft. Multipole analysis of the AMANDA-II neutrino skymap. Master's thesis, Rheinisch-Westfälische Technische Hochschule Aachen, 2009.

[20] The ROOT Team. TMath. http://root.cern.ch/root/html/TMath.html, 05.06.2012.

[21] The ROOT Team. TPrincipal. http://root.cern.ch/root/html/TPrincipal.html, 05.06.2012.

# Erklärung

Hiermit bestätige ich, dass ich diese Arbeit selbstständig und nur unter Verwendung der angegebenen Hilfsmittel angefertigt habe.

Erlangen,

03.09.2012